

Muon $g - 2$ and non-thermal leptogenesis in $U(1)_{L_\mu-L_\tau}$ model

Shintaro Eijima,^{1,*} Masahiro Ibe,^{1,2,†} and Kai Murai^{1,‡}

¹*ICRR, University of Tokyo, Kashiwa, Chiba 277-8582, Japan*

²*Kavli IPMU (WPI), UTIAS, University of Tokyo, Kashiwa, Chiba 277-8583, Japan*

Abstract

The gauged $U(1)_{L_\mu-L_\tau}$ symmetry is the simplest possibility to explain the observed muon $g - 2$, while being consistent with the neutrino oscillations through the seesaw mechanism. In this paper, we investigate if leptogenesis can work at the same time. At first glance, leptogenesis seems challenging because the right-handed neutrino masses are related to the $U(1)_{L_\mu-L_\tau}$ breaking scale of $10-100$ GeV as required from the muon $g - 2$. Contrary to this expectation, we find that non-thermal leptogenesis with the right-handed neutrino masses of $\mathcal{O}(10^7)$ GeV is possible. The successful scenario results in strict predictions on the neutrino oscillation parameters, which will be tested in future experiments.

* eijima@icrr.u-tokyo.ac.jp

† ibe@icrr.u-tokyo.ac.jp

‡ kmurai@icrr.u-tokyo.ac.jp

I. INTRODUCTION

The measurements of muon anomalous dipole moment at the Brookhaven National Laboratory [1] and at the Fermilab [2, 3] have reported the 4.2σ deviation from the Standard Model (SM) prediction [4].¹ One of the solutions to this anomaly is to introduce an extra, neutral gauge boson Z' associated with a gauged $U(1)$ symmetry. Its contribution through the gauge interaction can enlarge the muon $g - 2$. Taking into account the results in search experiments of Z' , the simplest remaining possibility is the $U(1)_{L_\mu-L_\tau}$ symmetry [27–33]. See Ref. [34] for the parameter space.

The gauge interaction of the $U(1)_{L_\mu-L_\tau}$ symmetry with leptons is given by

$$\mathcal{L}_{Z'} \supset -g_{Z'} Q_\alpha Z'_\kappa \left(L_\alpha^\dagger \bar{\sigma}^\kappa L_\alpha - \bar{l}_{R\alpha}^\dagger \bar{\sigma}^\kappa \bar{l}_{R\alpha} \right), \quad (1)$$

where $g_{Z'}$ is the gauge coupling constant, and $Q_{e,\mu,\tau} \equiv (0, +1, -1)$ are the charge of the $U(1)_{L_\mu-L_\tau}$ symmetry for each flavor. Here, $L_\alpha \equiv (\nu_{L\alpha}, l_{L\alpha})$ is the lepton doublet, and $\bar{l}_{R\alpha}$ is the singlet charged lepton with $\alpha = e, \mu, \tau$. Note that all the fermions are described by left-handed Weyl fermions. We follow the conventions of the spinor indices in Ref. [35]. The deviation of the muon $g - 2$ can be explained for $g_{Z'} \approx (3-10) \times 10^{-4}$ and the mass of Z' , $m_{Z'} \approx (1-20) \times 10$ MeV, while avoiding other experimental constraints [34]. This region corresponds to the $U(1)_{L_\mu-L_\tau}$ breaking scale of $10-100$ GeV.

Due to the $U(1)_{L_\mu-L_\tau}$ symmetry, neutrino oscillations can not occur. Even if the symmetry is broken, it is still non-trivial whether the observed neutrino oscillation parameters can be reproduced. In Refs. [36–38] (see also Refs. [39, 40] for earlier works), it has been shown that the type-I seesaw mechanism [41–46] with three right-handed neutrinos can explain the observed neutrino oscillations with $U(1)_{L_\mu-L_\tau}$ breaking scalar fields. Thus, the gauged $U(1)_{L_\mu-L_\tau}$ symmetry can explain the muon $g - 2$, while being consistent with the neutrino oscillations.

¹ For the theoretical prediction of the hadronic contributions to muon $g - 2$, see Refs. [5–24]. Currently, there are discrepancies between the data-driven approaches and the lattice simulations (see Ref. [25] and references therein). It has been also reported that a recent data-driven analysis shows deviation from the conventional results [26].

In this paper, we further investigate if leptogenesis can work while explaining the above two phenomena simultaneously. One can naively expect some obstacles to leptogenesis in this model. Firstly, masses of the right-handed neutrinos tend to be of the $U(1)_{L_\mu-L_\tau}$ breaking scale, $10-100$ GeV, to reproduce the neutrino oscillations by the seesaw mechanism. With such light right-handed neutrinos, thermal leptogenesis [47], for example, cannot be achieved. Secondly, in analogy to the electroweak symmetry breaking, the $U(1)_{L_\mu-L_\tau}$ symmetry seems to be restored in the early universe, and thus the universe is in the $U(1)_{L_\mu-L_\tau}$ symmetric phase before the freeze-out of sphaleron processes. As we will see, leptogenesis does not work in the symmetric phase. Therefore, to find a successful scenario of leptogenesis, we have to seek a setup satisfying the following conditions:

- Right-handed neutrinos have masses much larger than $10-100$ GeV.
- The $U(1)_{L_\mu-L_\tau}$ symmetry is broken even in the early universe.

We find that the first condition can be satisfied by a specific choice of Yukawa couplings of right-handed neutrinos to the $U(1)_{L_\mu-L_\tau}$ breaking fields, which in turn results in strict predictions on the neutrino oscillation parameters. The second condition can also be satisfied by choosing certain couplings between the $U(1)_{L_\mu-L_\tau}$ breaking scalar fields and the SM Higgs boson. Based on these outcomes, we demonstrate that non-thermal leptogenesis [48, 49] can generate a sufficient amount of baryon asymmetry while explaining the muon $g-2$ and the neutrino oscillations at the same time.

The rest of the paper is organized as follows. In Sec. II, we introduce a model with the gauged $U(1)_{L_\mu-L_\tau}$ symmetry and review the seesaw mechanism. In Sec. III, we discuss how heavy the right-handed neutrinos can be. In Sec. IV, we discuss restoration and breaking of the $U(1)_{L_\mu-L_\tau}$ symmetry in the early universe. In Sec. V, we discuss a possibility of leptogenesis in this model. Finally, we conclude this paper in Sec. VI.

II. MODEL WITH GAUGED $U(1)_{L_\mu-L_\tau}$ SYMMETRY

Let us start with the setup of the gauged $U(1)_{L_\mu-L_\tau}$ model which reproduces the active neutrino mass parameters [36, 37] (see also Refs. [39, 40] for earlier works). The $U(1)_{L_\mu-L_\tau}$ charge assignment for the doublet and the singlet leptons are given below Eq. (1). Three right-handed neutrinos are introduced to account for the neutrino oscillations via the type-I seesaw mechanism. They have the $U(1)_{L_\mu-L_\tau}$ charge as $(\bar{N}_e, \bar{N}_\mu, \bar{N}_\tau) = (0, -1, +1)$ in a natural way. Note again that all the fermions are described by left-handed Weyl fermions.

To break the $U(1)_{L_\mu-L_\tau}$ symmetry, we introduce two SM singlet scalar bosons $\sigma_{1,2}$ with the $U(1)_{L_\mu-L_\tau}$ charge +1 and +2, respectively. Note that the observed mixing angles among neutrinos can be reproduced by only σ_1 [36]. As we will see, however, σ_2 plays an important role in successful leptogenesis for the parameter region explaining the muon $g-2$. Hereafter, we call the sector consisting of Z' and $\sigma_{1,2}$ the $U(1)_{L_\mu-L_\tau}$ sector. We summarize the phenomenological properties of the symmetry breaking sector in the Appendix A.

The Lagrangian relating to the neutrino masses is given by

$$\begin{aligned} \mathcal{L}_\nu = & -y_L L_\alpha \Phi \bar{l}_{R\beta} - \lambda_\nu L_\alpha \tilde{\Phi} \bar{N}_\beta - \frac{M_R}{2} \bar{N}_\alpha \bar{N}_\beta - h_{e\mu} \sigma_1 \bar{N}_e \bar{N}_\mu - h_{e\tau} \sigma_1^* \bar{N}_e \bar{N}_\tau \\ & - \frac{1}{2} h_{\mu\mu} \sigma_2 \bar{N}_\mu \bar{N}_\mu - \frac{1}{2} h_{\tau\tau} \sigma_2^* \bar{N}_\tau \bar{N}_\tau + \text{h.c.} , \end{aligned} \quad (2)$$

where $\tilde{\Phi} = \epsilon \Phi$ is the Higgs doublet with the $SU(2)$ antisymmetric tensor ϵ . Due to the $U(1)_{L_\mu-L_\tau}$ symmetry, the Dirac Yukawa coupling constants and the Majorana mass matrix for right-handed neutrinos become

$$y_L = \begin{pmatrix} y_e & 0 & 0 \\ 0 & y_\mu & 0 \\ 0 & 0 & y_\tau \end{pmatrix}, \quad \lambda_\nu = \begin{pmatrix} \lambda_e & 0 & 0 \\ 0 & \lambda_\mu & 0 \\ 0 & 0 & \lambda_\tau \end{pmatrix}, \quad M_R = \begin{pmatrix} M_{ee} & 0 & 0 \\ 0 & 0 & M_{\mu\tau} \\ 0 & M_{\mu\tau} & 0 \end{pmatrix}, \quad (3)$$

where we choose y_α , λ_α , and $M_{\alpha\beta}$ are real and positive by rotating the phases of L 's, \bar{l}_R 's, and \bar{N} 's. We call $h_{\alpha\beta}$ Majorana Yukawa coupling constants.

When the $U(1)_{L_\mu-L_\tau}$ charged scalar fields obtain non-vanishing expectation values, $\langle\sigma_{1,2}\rangle$, the $U(1)_{L_\mu-L_\tau}$ symmetry is spontaneously broken. In the present model, both $\langle\sigma_{1,2}\rangle$ can be real positive (see the Appendix. A). In this case, Eq. (2) leads to the mass matrix of \bar{N}_α ,

$$M_{R,\text{eff}} = \begin{pmatrix} M_{ee} & h_{e\mu}\langle\sigma_1\rangle & h_{e\tau}\langle\sigma_1\rangle \\ h_{e\mu}\langle\sigma_1\rangle & h_{\mu\mu}\langle\sigma_2\rangle & M_{\mu\tau} \\ h_{e\tau}\langle\sigma_1\rangle & M_{\mu\tau} & h_{\tau\tau}\langle\sigma_2\rangle \end{pmatrix}. \quad (4)$$

The corresponding mass of the Z' boson is given by,

$$m_{Z'}^2 = 2g_{Z'}^2 (\langle\sigma_1\rangle^2 + 4\langle\sigma_2\rangle^2). \quad (5)$$

To explain the deviation of the muon $g-2$, we require, at the vacuum,

$$\sqrt{\langle\sigma_1\rangle_0^2 + 4\langle\sigma_2\rangle_0^2} \simeq 10-100 \text{ GeV}, \quad (6)$$

(see Fig. 1). As we will discuss later, the temperature-dependent expectation values play important roles in successful leptogenesis. Thus, we put the subscript 0 on the vacuum expectation value (VEV) to distinguish it from the temperature-dependent expectation value. The complex scalar field σ_2 is absent in the minimal model in Refs. [36–38]. In that case, the mass matrix is reduced to the so-called two-zero minor [50, 51].

The active neutrino masses are given by the seesaw mechanism;

$$M_\nu \simeq -M_D M_{R,\text{eff}}^{-1} M_D^T, \quad M_D \equiv \lambda_\nu v_{\text{EW}}, \quad (7)$$

where v_{EW} denotes the electroweak symmetry breaking scale, $\langle\Phi\rangle_0 = v_{\text{EW}} \simeq 174 \text{ GeV}$. Note that $\langle\sigma_{1,2}\rangle_0 \neq 0$ contribution is crucial to explain the observed neutrino oscillations since otherwise $M_{R,\text{eff}}$ induces only a mixing angle θ_{23} between the active neutrinos. As we will see in the next section, even for $\langle\sigma_{1,2}\rangle_0 \neq 0$, the mass parameters M_{ee} and $M_{\mu\tau}$ are severely constrained to reproduce the observed neutrino oscillations.

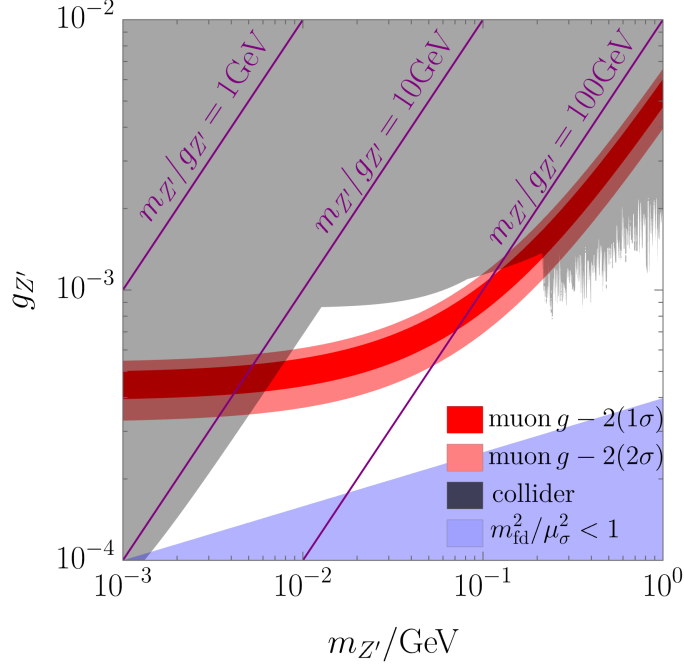


Figure 1. Parameter region that explains the muon $g - 2$ within the 1σ (red) and the 2σ (pink) ranges [2]. We show $m_{Z'}/g_{Z'}$ by the purple lines, which indicate the size of the VEVs of the scalar fields. The gray shaded region is excluded by the neutrino trident production experiment [52], the neutrino-electron scattering experiments [53, 54], and the experiment searching for $e^-e^+ \rightarrow \mu^-\mu^+Z'$ [55]. In the blue shaded region, the ratio $m_{\text{fd}}^2/\mu_\sigma^2 < 1$ for $T = T_{\text{th}}$ in Eq. (40) (see Sec. IV A).

For later purposes, it is useful to consider $\lambda_\nu^{-1} M_{R,\text{eff}} \lambda_\nu^{-1}$, which is related to the low energy observables via,

$$\begin{pmatrix} \frac{M_{ee}}{\lambda_e^2} & \frac{h_{e\mu}\langle\sigma_1\rangle_0}{\lambda_e\lambda_\mu} & \frac{h_{e\tau}\langle\sigma_1\rangle_0}{\lambda_e\lambda_\tau} \\ \frac{h_{e\mu}\langle\sigma_1\rangle_0}{\lambda_e\lambda_\mu} & \frac{h_{\mu\mu}\langle\sigma_2\rangle_0}{\lambda_\mu^2} & \frac{M_{\mu\tau}}{\lambda_\mu\lambda_\tau} \\ \frac{h_{e\tau}\langle\sigma_1\rangle_0}{\lambda_e\lambda_\tau} & \frac{M_{\mu\tau}}{\lambda_\mu\lambda_\tau} & \frac{h_{\tau\tau}\langle\sigma_2\rangle_0}{\lambda_\tau^2} \end{pmatrix} = v_{\text{EW}}^2 \times \text{U}[M_\nu^d]^{-1}\text{U}^T, \quad (8)$$

where M_ν^d is a diagonal mass matrix defined by $M_\nu^d \equiv \text{U}^T M_\nu \text{U}$ with the Pontecorvo-Maki-Nakagawa-Sakata (PMNS) matrix U . Here, M_ν is invertible, and thus all the active neutrinos become massive. The PMNS matrix is represented by the mixing angles $\theta_{12}, \theta_{23}, \theta_{13}$, the

Dirac CP phase δ , and the Majorana CP phases η_1, η_2 as

$$\begin{aligned}
U &= \begin{pmatrix} 1 & 0 & 0 \\ 0 & c_{23} & s_{23} \\ 0 & -s_{23} & c_{23} \end{pmatrix} \begin{pmatrix} c_{13} & 0 & s_{13}e^{-i\delta} \\ 0 & 1 & 0 \\ -s_{13}e^{i\delta} & 0 & c_{13} \end{pmatrix} \begin{pmatrix} c_{12} & s_{12} & 0 \\ -s_{12} & c_{12} & 0 \\ 0 & 0 & 1 \end{pmatrix} \begin{pmatrix} 1 & 0 & 0 \\ 0 & e^{i\eta_1/2} & 0 \\ 0 & 0 & e^{i\eta_2/2} \end{pmatrix} \\
&= \begin{pmatrix} c_{12}c_{13} & s_{12}c_{13} & s_{13}e^{-i\delta} \\ -s_{12}c_{23} - c_{12}s_{23}s_{13}e^{i\delta} & c_{12}c_{23} - s_{12}s_{23}s_{13}e^{i\delta} & s_{23}c_{13} \\ s_{12}s_{23} - c_{12}c_{23}s_{13}e^{i\delta} & -c_{12}s_{23} - s_{12}c_{23}s_{13}e^{i\delta} & c_{23}c_{13} \end{pmatrix} \begin{pmatrix} 1 & 0 & 0 \\ 0 & e^{i\eta_1/2} & 0 \\ 0 & 0 & e^{i\eta_2/2} \end{pmatrix}, \quad (9)
\end{aligned}$$

where s_{ij} and c_{ij} denote $\sin\theta_{ij}$ and $\cos\theta_{ij}$, respectively.² The domains of the mixing angles are in $[0, \pi/2)$, while those of the CP phases are in $[0, 2\pi)$. We should note that, in this model, there are no additional CP phases in the lepton sector other than δ , η_1 , and η_2 .

III. HOW HEAVY CAN THE RIGHT-HANDED NEUTRINOS BE?

In this section, we consider possible ranges of the mass parameters of the right-handed neutrinos that reproduce the neutrino oscillations. As a reference, we summarize the observed oscillation parameters in Tab. I. As the mixing angles of the active neutrinos are of $\mathcal{O}(1)$, we naively expect that M_{ee} and $M_{\mu\tau}$ should be $\mathcal{O}(\langle\sigma_{1,2}\rangle_0)$. Thus, in order to explain the muon $g-2$ and the neutrino oscillations at the same time, M_{ee} and $M_{\mu\tau}$ are expected to be 10–100 GeV.

Surprisingly, however, we find that both M_{ee} and $M_{\mu\tau}$ can be as large as $\mathcal{O}(10^7)$ GeV for special cases where the active neutrino masses are degenerate. Such large right-handed neutrino mass parameters open up possibilities for leptogenesis by the decay of right-handed neutrinos.

² The above PMNS matrix corresponds to the old PDG convention [56].

Table I. Three-flavor oscillation parameters by NuFIT 5.1 [57]^a with the data on atmospheric neutrinos by the Super-Kamiokande collaboration.

	Normal Ordering		Inverted Ordering	
	best fit point	3σ range	best fit point	3σ range
$\sin^2 \theta_{12}$	0.304	$0.269 \rightarrow 0.343$	0.304	$0.269 \rightarrow 0.343$
$\sin^2 \theta_{23}$	0.450	$0.408 \rightarrow 0.603$	0.570	$0.410 \rightarrow 0.613$
$\sin^2 \theta_{13}$	0.02246	$0.02060 \rightarrow 0.02435$	0.02241	$0.02055 \rightarrow 0.02457$
$\Delta m_{21}^2 [10^{-5} \text{ eV}^2]$	7.42	$6.82 \rightarrow 8.04$	7.42	$6.82 \rightarrow 8.04$
$\Delta m_{3l}^2 [10^{-3} \text{ eV}^2]$	2.510	$2.430 \rightarrow 2.593$	-2.490	$-2.574 \rightarrow -2.410$
$\delta [^\circ]$	230	$144 \rightarrow 350$	278	$194 \rightarrow 345$

^a <http://www.nu-fit.org/>

A. Non-degenerate active neutrino masses

First, let us consider the case where the active neutrino masses are not degenerate. Especially, we assume that the lightest active neutrino mass m_l is much smaller than $\sqrt{\Delta m_{\text{sol/atm}}^2}$. In this case, the right hand side of Eq. (8) is given by

$$v_{\text{EW}}^2 \times (\mathbf{U}[M_\nu^d]^{-1}\mathbf{U}^T)_{\alpha\beta} = \frac{v_{\text{EW}}^2}{m_l} \times \left[\mathbf{U}_{\alpha l} \mathbf{U}_{\beta l} + \mathcal{O} \left(\frac{m_l}{\sqrt{\Delta m_{\text{sol/atm}}^2}} \right) \right], \quad (10)$$

where l is the index corresponding to the lightest active neutrino. For the central values of the neutrino mixing parameters in both of the normal and inverted orderings, the sizes of $\mathbf{U}_{\alpha l} \mathbf{U}_{\beta l}$ are at least of $\mathcal{O}(0.01)$. In the limit of $m_l \ll \sqrt{\Delta m_{\text{sol/atm}}^2}$, the first term in Eq. (10) is dominant. Then, we can obtain a constraint on the mass parameters by comparing the product of (1, 1) and (2, 3) elements and that of (1, 2) and (1, 3) elements of Eq. (8). We can also obtain another constraint by comparing the product of (2, 2) and (3, 3) elements and

that of (2, 3) and (3, 2) elements of Eq. (8). As a result, we find

$$\frac{M_{ee}M_{\mu\tau}}{h_{e\mu}h_{e\tau}\langle\sigma_1\rangle_0^2} \sim 1 , \quad (11)$$

$$\frac{M_{\mu\tau}^2}{h_{\mu\mu}h_{\tau\tau}\langle\sigma_2\rangle_0^2} \sim 1 , \quad (12)$$

where we roughly take all the elements of $U_{\alpha l}U_{\beta l} \sim 1$. These constraints are independent of the Dirac Yukawa couplings, λ_α 's. It can be read that these constraints are valid for $m_l \lesssim 0.01\sqrt{\Delta m_{\text{sol/atm}}^2}$.

From the second constraint, we find that $M_{\mu\tau}$ is at most of $\mathcal{O}(\langle\sigma_2\rangle_0)$. On the other hand, M_{ee} can be as large as $\langle\sigma_1\rangle_0^2/M_{\mu\tau}$, which is much larger than $\langle\sigma_1\rangle_0$ when $M_{\mu\tau}$ is much smaller than $\langle\sigma_1\rangle_0$.

B. Quasi-degenerate active neutrino masses in the normal ordering

As shown above, the combinations of the elements in Eq. (8) lead to constraints on the mass parameters. Here, we consider the case where some elements in Eq. (8) vanish and both M_{ee} and $M_{\mu\tau}$ can be much larger than $\langle\sigma_{1,2}\rangle_0$.

First, we focus on the normal ordering. In this case, the active neutrino masses are given by

$$m_1 = m_l , \quad m_2 = \sqrt{m_l^2 + \Delta m_{\text{sol}}^2} , \quad m_3 = \sqrt{m_l^2 + \Delta m_{\text{atm}}^2} . \quad (13)$$

From the CMB observations, the sum of the active neutrino masses is constrained as $\sum m_i < 0.26$ eV at the 95% C.L. [58], which means $m_l \lesssim 0.082$ eV. (When the CMB lensing and the BAO are included, it becomes $\sum m_i < 0.12$ eV, which means $m_l \lesssim 0.030$ eV.) As seen above, M_{ee} and $M_{\mu\tau}$ are tied to $\langle\sigma_{1,2}\rangle_0$ if $m_l \ll \sqrt{\Delta m_{\text{sol/atm}}^2}$. To liberate M_{ee} and $M_{\mu\tau}$ from $\langle\sigma_{1,2}\rangle_0$, we consider m_l comparable to $\sqrt{\Delta m_{\text{atm}}^2}$.

As an example, we fix $m_l = 0.06$ eV and adopt the center values for $\Delta m_{\text{sol/atm}}^2$ and the

following mixing angles:

$$\begin{aligned}\Delta m_{\text{sol}}^2 &= 7.42 \times 10^{-5} \text{ eV}^2, & \Delta m_{\text{atm}}^2 &= 2.510 \times 10^{-3} \text{ eV}^2, \\ \sin^2 \theta_{12} &= 0.304, & \sin^2 \theta_{13} &= 0.02246.\end{aligned}\tag{14}$$

We also take the rest of the oscillation parameters as

$$\sin^2 \theta_{23} \simeq 0.565, \quad \delta \simeq 268^\circ, \quad \eta_1 \simeq 355^\circ, \quad \eta_2 \simeq 177^\circ,\tag{15}$$

where θ_{23} and δ are in the 2σ ranges of the observational data [57]. In this case, the (1, 2) and (2, 2) elements of Eq. (8) vanish:³

$$v_{\text{EW}}^2 \times \mathbf{U}[\mathbf{M}_\nu^d]^{-1} \mathbf{U}^T \simeq \frac{v_{\text{EW}}^2}{m_l} \times \begin{pmatrix} 0.99 e^{-0.03i} & 0 & 0.05 e^{1.4i} \\ 0 & 0 & 0.88 e^{3.1i} \\ 0.05 e^{1.4i} & 0.88 e^{3.1i} & 0.22 e^{-0.05i} \end{pmatrix}.\tag{16}$$

This structure corresponds to $h_{e\mu} = h_{\mu\mu} = 0$. Note also that this zero texture can be achieved with the opposite CP phases (mod 2π), although the corresponding Dirac CP phase is disfavored by observations [57].

With this structure of Eq. (16), the mass parameters and $\langle \sigma_{1,2} \rangle_0$ are related as

$$\frac{M_{ee}}{\lambda_e^2} \sim \frac{M_{\mu\tau}}{\lambda_\mu \lambda_\tau} \sim \frac{h_{e\tau} \langle \sigma_1 \rangle_0}{\lambda_e \lambda_\tau} \sim \frac{h_{\tau\tau} \langle \sigma_2 \rangle_0}{\lambda_\tau^2} \sim \frac{v_{\text{EW}}^2}{m_l} \equiv M_s \simeq 5 \times 10^{14} \text{ GeV}.\tag{17}$$

From this relation, we obtain

$$M_{\mu\tau} \sim \lambda_\mu h_{e\tau} \langle \sigma_1 \rangle_0 \sqrt{\frac{M_s}{M_{ee}}}.\tag{18}$$

³ Here, we numerically find a parameter set in Eq. (15) where the (1, 2) and (2, 2) elements of Eq. (8) are suppressed by a factor of $\mathcal{O}(10^{-13})$ compared with the other elements by varying $(\theta_{23}, \delta, \eta_1, \eta_2)$. Thus, strictly speaking, the (1, 2) and (2, 2) elements might not vanish exactly. In this case, the constraints on the mass parameters in Eqs. (11) and (12) are relaxed by this factor, and the mass spectrum discussed in the following can be realized. This is also true for the case of the inverted ordering discussed below.

If $\lambda_\mu \simeq 1$, $h_{e\tau} \simeq 1$, $\langle\sigma_1\rangle_0 \simeq 100 \text{ GeV}$, the mass parameters takes the maximum values as

$$M_{\mu\tau} \sim 10^6 \text{ GeV} \left(\frac{M_{ee}}{5 \times 10^6 \text{ GeV}} \right)^{-1/2}, \quad (19)$$

which is a rough estimate ignoring coefficients of $\mathcal{O}(0.01)$ in Eq. (16). Note that, even if one of λ_α 's is unity, these choices satisfy the constraints from the charged flavor violation such as $\mu \rightarrow e + \gamma$ [59] or $\tau \rightarrow e + \gamma$ [60] due to the smallness of the other λ_α 's.

For the normal ordering, it is also possible that both (2, 2) and (3, 3) elements in Eq. (8) vanish with specific choices of the lightest active neutrino mass and mixing parameters. This case is nothing but the minimal gauged $U(1)_{L_\mu-L_\tau}$ model without σ_2 studied in Refs. [37, 38]. For this structure, however, the mass parameters are still constrained as Eq. (11) and either of M_{ee} and $M_{\mu\tau}$ is smaller than the scale of $\langle\sigma_1\rangle_0$.

At the end of this subsection, we comment on the constraints on the effective neutrino mass for the neutrinoless double beta ($0\nu\beta\beta$) decay,

$$m_{\beta\beta} \equiv \left| \sum_i m_i U_{ei}^2 \right|. \quad (20)$$

$m_{\beta\beta}$ is bounded through the upper bound on the lifetime of the $0\nu\beta\beta$ decay from the KamLAND-Zen [61] and GERDA [62] experiments as

$$m_{\beta\beta} < 36 - 156 \text{ meV}, \quad (21)$$

$$m_{\beta\beta} < 79 - 180 \text{ meV}, \quad (22)$$

respectively. The uncertainties of the upper bound come from the variety of nuclear matrix element calculations. For our parameter choice, we obtain

$$m_{\beta\beta} \simeq 61 \text{ meV}, \quad (23)$$

which is consistent with the current constraints of the $0\nu\beta\beta$ decay experiments.

C. Quasi-degenerate active neutrino masses in the inverted ordering

Next, we consider the inverted ordering. In this case, the active neutrino masses are given by

$$m_1 = \sqrt{m_l^2 + \Delta m_{\text{atm}}^2 - \Delta m_{\text{sol}}^2}, \quad m_2 = \sqrt{m_l^2 + \Delta m_{\text{atm}}^2}, \quad m_3 = m_l. \quad (24)$$

For this mass spectrum, the cosmological constraint $\sum m_i < 0.26 \text{ eV}$ [58] corresponds to $m_l \lesssim 0.077 \text{ eV}$. We again consider m_l comparable to $\sqrt{\Delta m_{\text{atm}}^2}$ and fix

$$m_l = 0.06 \text{ eV}, \quad \Delta m_{\text{sol}}^2 = 7.42 \times 10^{-5} \text{ eV}^2, \quad \Delta m_{\text{atm}}^2 = 2.490 \times 10^{-3} \text{ eV}^2, \\ \sin^2 \theta_{12} = 0.304, \quad \sin^2 \theta_{13} = 0.02241. \quad (25)$$

In this case, we find that the (1, 3) and (3, 3) elements of Eq. (8) vanish as

$$v_{\text{EW}}^2 \times \mathbf{U}[M_\nu^d]^{-1} \mathbf{U}^T \simeq \frac{v_{\text{EW}}^2}{m_l} \times \begin{pmatrix} 0.78 e^{-0.03i} & 0.05 e^{-1.7i} & 0 \\ 0.05 e^{-1.7i} & 0.23 e^{3.1i} & 0.88 e^{3.1i} \\ 0 & 0.88 e^{3.1i} & 0 \end{pmatrix}, \quad (26)$$

for

$$\sin^2 \theta_{23} = 0.566, \quad \delta \simeq 270^\circ, \quad \eta_1 \simeq 355^\circ, \quad \eta_2 \simeq 177^\circ, \quad (27)$$

where θ_{23} and δ are in the 1σ ranges of the observational data [57]. This structure corresponds to $h_{e\tau} = h_{\tau\tau} = 0$. As in the case of the normal ordering, this zero texture can be achieved with the opposite CP phases in spite of a disfavored Dirac CP phase.

Since the structure of Eq. (26) is the same as that of Eq. (16) except for the replacement of $\mu \leftrightarrow \tau$, we obtain the estimate of

$$M_{\mu\tau} \sim \lambda_\mu h_{e\mu} \langle \sigma_1 \rangle_0 \sqrt{\frac{M_s}{M_{ee}}}. \quad (28)$$

Thus, for $\lambda_\tau \simeq 1$, $h_{e\mu} \simeq 1$, $\langle \sigma_1 \rangle_0 \simeq 100 \text{ GeV}$, the mass parameters take the maximum values

as in Eq. (19).

For this parameter choice, the effective neutrino mass of $0\nu\beta\beta$ decay is

$$m_{\beta\beta} \simeq 77 \text{ meV} , \quad (29)$$

which is consistent with the current constraints of the $0\nu\beta\beta$ decay experiments.

IV. BREAKING OF THE $U(1)_{L_\mu-L_\tau}$ SYMMETRY IN THE EARLY UNIVERSE

As we will see in the next section, successful leptogenesis requires non-vanishing expectation values of $\sigma_{1,2}$, and hence, it is important to clarify the aspects of the $U(1)_{L_\mu-L_\tau}$ symmetry breaking in the early universe.

In section II, we introduced two $U(1)_{L_\mu-L_\tau}$ charged scalars. To discuss the nature of symmetry breaking, it is enough to consider a single $U(1)_{L_\mu-L_\tau}$ charged scalar σ . A tree-level Lagrangian for σ and the SM Higgs doublet Φ is given by

$$\begin{aligned} \mathcal{L}_{\sigma,\Phi} &= |D_\mu \sigma|^2 + |D_\mu \Phi|^2 - V(\sigma, \Phi) , \\ V(\sigma, \Phi) &= -\mu_\sigma^2 |\sigma|^2 - \mu_\Phi^2 \Phi^\dagger \Phi + \lambda_\sigma |\sigma|^4 + \lambda_\Phi (\Phi^\dagger \Phi)^2 + \lambda_{\Phi\sigma} |\sigma|^2 (\Phi^\dagger \Phi) , \end{aligned} \quad (30)$$

where μ_σ^2, μ_Φ^2 express mass parameters for each scalar field, $\lambda_\sigma, \lambda_\Phi$ are quartic self-couplings, and $\lambda_{\Phi\sigma}$ is a Higgs- σ coupling. In the following, we take $\mu_\Phi^2, \lambda_\sigma$ and λ_Φ positive. The covariant derivative on σ is given by, $D_\kappa = \partial_\kappa + ig_{Z'} Q_{L_\mu-L_\tau} Z'_\kappa$, while Φ has no $U(1)_{L_\mu-L_\tau}$ charge.

At low energy, the electroweak symmetry is broken by the VEV of Φ , and hence, the mass term of σ around $\sigma = 0$ is given by,

$$-\mu_0^2 |\sigma|^2 \equiv -(\mu_\sigma^2 - \lambda_{\Phi\sigma} v_{\text{EW}}^2) |\sigma|^2 . \quad (31)$$

Since we require that the $U(1)_{L_\mu-L_\tau}$ symmetry is broken at the vacuum, we take $\mu_0^2 > 0$.

The resultant VEV of σ is given by,

$$\langle \sigma \rangle_0 = \frac{\mu_0}{\sqrt{2\lambda_\sigma}} , \quad (32)$$

where we take $\langle \sigma \rangle_0$ real and positive without loss of generality.

A. Symmetry restoration by thermal/finite density effects

Let us consider the symmetry restoration in the early universe. In this subsection, we neglect $\lambda_{\Phi\sigma}$ for a while, and hence, $\mu_0^2 = \mu_\sigma^2 > 0$. In the early universe, σ obtains an effective mass term as $V_{\text{eff}} = m_{\text{eff}}^2 |\sigma|^2$, which depends on environment such as thermal bath. For $m_{\text{eff}}^2 > \mu_0^2$, the $U(1)_{L_\mu-L_\tau}$ symmetry breaking does not occur. Therefore, we find the cosmic temperature $T = T_c$ at which the phase of the $U(1)_{L_\mu-L_\tau}$ symmetry changes, that is, $m_{\text{eff}}^2|_{T_c} = \mu_0^2$. Note that μ_0 is bounded from above to explain the muon $g-2$ as $\mu_0 = \sqrt{2\lambda_\sigma} \langle \sigma \rangle_0 \lesssim 100 \text{ GeV}$. First, let us evaluate the effective mass squared in the environment where the $U(1)_{L_\mu-L_\tau}$ sector is thermalized by the $U(1)_{L_\mu-L_\tau}$ gauge interaction with SM particles in the thermal bath.

The rate of the gauge interaction is given by $\Gamma_g \approx (g_{Z'}^4/4\pi)T$ for $T \gg m_{Z'}$. Then, we obtain the thermalization temperature as

$$T_{\text{th}} \approx 6 \times 10^4 \text{ GeV} \left(\frac{g_{Z'}}{10^{-3}} \right)^4 , \quad (33)$$

where the interaction rate Γ_g becomes equal to the Hubble expansion rate H . For $T < T_{\text{th}}$, the $U(1)_{L_\mu-L_\tau}$ sector is thermalized. The Hubble rate is given by $H = \sqrt{\pi^2 g_*/90} T^2 / M_P$, where M_P is the reduced Planck scale and $g_* \sim 100$ is the effective degrees of freedom of the relativistic species.

When the $U(1)_{L_\mu-L_\tau}$ sector is thermalized, the thermal mass is given by

$$m_{\text{eff}}^2 = \left(\frac{\lambda_\sigma}{3} + \frac{g_{Z'}^2}{8} \right) T^2 > 0. \quad (34)$$

At high temperatures where the thermal mass is larger than μ_0^2 , the $U(1)_{L_\mu-L_\tau}$ symmetry is in the symmetric phase. Decreasing the temperature, the symmetry breaking takes place at the breaking temperature,

$$T_{\text{bre}} = \left(\frac{\lambda_\sigma}{3} + \frac{g_{Z'}^2}{8} \right)^{-1/2} \mu_0 \simeq \langle \sigma \rangle_0 = 10 - 100 \text{ GeV} . \quad (35)$$

Therefore, the $U(1)_{L_\mu-L_\tau}$ symmetry is in the symmetric phase for at least $T_{\text{bre}} < T < T_{\text{th}}$.

Next, let us move on to higher temperatures, $T > T_{\text{th}}$, where the $U(1)_{L_\mu-L_\tau}$ sector is not thermalized and σ does not obtain the thermal mass. Even in this case, σ has an effective mass squared, $m_{\text{eff}}^2 = m_{\text{fd}}^2$, due to the finite density effect of the non-thermalized $U(1)_{L_\mu-L_\tau}$ sector particles, which are produced from the SM thermal bath. As derived in the Appendix B, it is given by

$$m_{\text{fd}}^2 = C_X n_X \langle p_X^{-1} \rangle, \quad (36)$$

where n_X and p_X are the number density and momentum of a particle X that interacts with σ , respectively, and C_X is a coefficient depending on the interaction. Here, $\langle \rangle$ expresses the averaged value over the particle distribution.

To evaluate m_{fd}^2 from the self-interaction of σ , we estimate the number density of σ , n_σ . For the production of σ , *e.g.*, $\mu\bar{\mu} \rightarrow \sigma\sigma^*$, n_σ follows the Boltzmann equation,

$$\frac{dn_\sigma}{dt} + 3Hn_\sigma = \langle \sigma v \rangle n_\mu^2, \quad (37)$$

where the cross section is given by $\langle \sigma v \rangle \sim g_{Z'}^4/(4\pi T^2)$, and $n_\mu = (3\zeta(3)/2\pi^2)T^3$. For $T > T_{\text{th}}$, n_σ is given by

$$n_\sigma = \kappa \frac{g_{Z'}^4}{4\pi} M_P T^2, \quad (38)$$

where κ is a numerical $\mathcal{O}(1)$ factor. For the self-interaction of σ in Eq. (30), the effective

mass squared can be read as

$$m_{\text{fd}}^2 \simeq \lambda_\sigma n_\sigma \langle p_\sigma^{-1} \rangle \simeq \kappa \frac{\lambda_\sigma g_{Z'}^4}{4\pi} M_P T, \quad (39)$$

where we use $\langle p_\sigma^{-1} \rangle \simeq T^{-1}$ since σ is produced from the SM thermal bath.

Compared with the tree-level mass squared μ_σ^2 ,

$$\frac{m_{\text{fd}}^2(T)}{\mu_\sigma^2} \simeq 2 \times 10^6 \kappa \left(\frac{50 \text{ GeV}}{\mu_\sigma / \sqrt{2\lambda_\sigma}} \right)^2 \left(\frac{g_{Z'}}{10^{-3}} \right)^8 \left(\frac{T}{T_{\text{th}}} \right), \quad (40)$$

for $T > T_{\text{th}}$. In Fig. 1, we show the parameter region where $m_{\text{fd}}^2(T_{\text{th}})/\mu_\sigma^2 < 1$ as a blue shaded region.⁴ The figure shows that $m_{\text{fd}}^2(T_{\text{th}})/\mu_\sigma^2 > 1$ for the parameter region that explains the muon $g - 2$, and hence, we find that the $U(1)_{L_\mu - L_\tau}$ symmetry is restored even at the temperature above T_{th} . As a result, we find that the symmetry is preserved at $T > T_{\text{bre}}$ by combining the results from the thermal and finite density effects.

We should discuss here how restoration of the symmetry proceeds when the initial condition of the universe is in the $U(1)_{L_\mu - L_\tau}$ broken phase. Let us suppose that the $U(1)_{L_\mu - L_\tau}$ charged scalar field is initially settled at $\sigma \sim \langle \sigma \rangle_0$ and the scalar potential arises as $V(\sigma) \sim m_{\text{fd}}^2 |\sigma|^2$ just after reheating of the universe. In this situation, we can consider that σ rapidly moves to $\sigma = 0$ if

$$m_{\text{fd}}^2 > H^2. \quad (41)$$

By using Eq. (39), it turns out that the symmetry is restored immediately when the following condition is satisfied;

$$T < T_{\text{rest}} \simeq \left(\frac{\lambda_\sigma g_{Z'}^4}{4\pi} \right)^{\frac{1}{3}} M_P \simeq 10^{14} \text{ GeV} \lambda_\sigma^{1/3} \left(\frac{g_{Z'}}{10^{-3}} \right)^{4/3}. \quad (42)$$

Thus, even if the $U(1)_{L_\mu - L_\tau}$ symmetry is initially broken with $\sigma \sim \langle \sigma \rangle_0$, it is restored at the temperature relevant to the following discussion.

⁴ We assume that $\lambda_\sigma \gg g_{Z'}^2 = \mathcal{O}(10^{-6})$, and then the effective mass squared is mainly contributed by the self-interaction of σ . In the figure, we take $\lambda_{\Phi\sigma} = 0$, and hence $\mu_\sigma / \sqrt{2\lambda_\sigma} = m_{Z'} / \sqrt{2} g_{Z'}$.

B. Symmetry breaking by thermal effects

So far, we have concentrated on the effects of the $U(1)_{L_\mu-L_\tau}$ gauge interaction and the self-interaction of σ , which restores the $U(1)_{L_\mu-L_\tau}$ symmetry at $T > T_{\text{bre}}$. The aspects of the $U(1)_{L_\mu-L_\tau}$ symmetry breaking, however, drastically change when the Higgs- σ coupling $\lambda_{\Phi\sigma}$ takes a certain negative value.⁵ In the presence of a sizable $\lambda_{\Phi\sigma}$, σ is thermalized through the interaction with Φ . Then, the effective scalar potential of σ obtains a contribution from the Higgs- σ interaction,

$$V(\sigma) \sim -|\lambda_{\Phi\sigma}|T^2 \times |\sigma|^2, \quad (43)$$

where we omit a numerical coefficient. For $|\lambda_{\Phi\sigma}| \gg \lambda_\sigma, g_{Z'}^2$, the thermal mass is dominated by this contribution. As a result, σ acquires a non-zero expectation value,

$$\langle \sigma \rangle \sim \sqrt{|\lambda_{\Phi\sigma}|/\lambda_\sigma} T, \quad (44)$$

and thus the $U(1)_{L_\mu-L_\tau}$ symmetry is broken even at high temperatures.

Several comments are in order. Firstly, note that the relative sizes of λ_Φ , λ_σ , and $|\lambda_{\Phi\sigma}|$ are constrained by the unbounded-from-below condition, $|\lambda_{\Phi\sigma}| < 2\sqrt{\lambda_\Phi\lambda_\sigma}$. Under this constraint, the back-reaction of $\langle \sigma \rangle$ to the Higgs potential, *i.e.*, $\lambda_{\Phi\sigma}\langle \sigma \rangle^2|\Phi|^2$ is at most $\lambda_\Phi T^2|\Phi|^2$. It is subdominant compared with the top Yukawa contributions, and thus the back-reaction does not affect the dynamics of the electroweak sector significantly. Incidentally, we also find the thermal mass of Φ through the σ -loop is negligible due to $|\lambda_{\Phi\sigma}| \ll \lambda_\Phi$ for $|\lambda_{\Phi\sigma}| \gg \lambda_\sigma$.

Secondly, note that σ and Z' do not affect the standard cosmology below $T < \mathcal{O}(m_{Z'})$. To see this, we denote the mass eigenstates of the physical components in Φ and σ by H and S . The modulus of the Higgs boson Φ_0 contains H and S as $\Phi_0 = (H \cos \theta + S \sin \theta)/\sqrt{2}$ with a mixing angle θ . We take H to be the observed Higgs boson so that $m_H \simeq 125 \text{ GeV}$, while the mass of S , m_S , is smaller.⁶ We assume $\lambda_\sigma \gg g_{Z'}^2$ and then $m_S \gg m_{Z'}$. In this

⁵ In the following, we will take $|\lambda_{\Phi\sigma}| < \mathcal{O}(10^{-2})$. Then, the VEVs of Φ and σ do not significantly affect each other while $\lambda_{\Phi\sigma} < 0$ plays an important role at high temperatures. Moreover, $\mu_0 \simeq \mu_\sigma$ is justified for this range of $\lambda_{\Phi\sigma}$, and the blue shaded region in Fig. 1, $m_{\text{fd}}^2/\mu_\sigma^2 < 1$, is still valid.

⁶ In the model discussed in the previous section, we have two complex scalars σ_1 and σ_2 . The discussion in the present section is given in the Appendix A.

limit, S decays into a pair of the longitudinal mode of Z' immediately (see the Appendix A). As Z' also decays immediately into a pair of neutrinos, Z' and σ do not cause cosmological problems for $m_S \gg m_{Z'} \gg \mathcal{O}(1) \text{ MeV}$ (see Ref. [63]).

Finally, we also comment on the experimental constraints on $|\lambda_{\Phi\sigma}|$. In the model discussed in the previous section, we introduced two scalars, σ_1 and σ_2 , that couple to Φ through $\lambda_{\Phi\sigma_1}$ and $\lambda_{\Phi\sigma_2}$, respectively. As we see in the Appendix A, the upper limit on the branching fraction of Higgs invisible decay mode, $\text{Br}(H \rightarrow \text{invisible}) < 0.11$ [64], leads to

$$(|\lambda_{\Phi\sigma_1}|^2 + |\lambda_{\Phi\sigma_2}|^2)^{1/2} < 7 \times 10^{-3} , \quad (45)$$

(see also Ref. [65]).

V. LEPTOGENESIS IN THE $U(1)_{L_\mu-L_\tau}$ MODEL

We first consider a leptogenesis scenario with a negligible $\lambda_{\Phi\sigma}$. In this case, as seen in the previous section, the $U(1)_{L_\mu-L_\tau}$ symmetry is not broken at $T > T_{\text{bre}} = 10 - 100 \text{ GeV}$. This temperature is lower than the temperature where sphaleron processes freeze out, $T_{\text{sph}} \approx 130 \text{ GeV}$.⁷ Since leptogenesis requires that the sphaleron processes convert the lepton asymmetry into the baryon asymmetry, we need to consider leptogenesis in the $U(1)_{L_\mu-L_\tau}$ symmetric phase. As we will see shortly, however, leptogenesis does not occur in the $U(1)_{L_\mu-L_\tau}$ symmetric phase.

On the other hand, when we consider a sizable $\lambda_{\Phi\sigma} < 0$, the $U(1)_{L_\mu-L_\tau}$ symmetry is broken in the early universe. In this case, we find that the non-thermal leptogenesis [48, 49] can generate sufficient lepton asymmetry to explain the observed baryon asymmetry of the universe.

⁷ There could be a region where $T_{\text{bre}} \gtrsim T_{\text{sph}}$ in a corner of the parameter space of Z' to explain the muon $g - 2$. In this case, the $U(1)_{L_\mu-L_\tau}$ symmetry breaking takes place before the sphaleron processes freeze out. Although this leaves a possibility of the leptogenesis scenarios at around T_{sph} , it is beyond the scope of this paper.

A. Failures of leptogenesis in the $U(1)_{L_\mu-L_\tau}$ symmetric phase

To discuss leptogenesis in the $U(1)_{L_\mu-L_\tau}$ symmetric phase, it is convenient to construct a Dirac fermion from the two left-handed Weyl fermions, \bar{N}_μ and \bar{N}_τ ,

$$\Psi_{\mu\tau} \equiv \begin{pmatrix} \bar{N}_\mu \\ \bar{N}_\tau^\dagger \end{pmatrix}, \quad (46)$$

which has a $U(1)_{L_\mu-L_\tau}$ charge -1 . In the symmetric phase, $M_{\mu\tau}$ provides the Dirac mass term of $\Psi_{\mu\tau}$. The remaining right-handed neutrino forms a four-component Majorana fermion,

$$\Psi_e \equiv \begin{pmatrix} \bar{N}_e \\ \bar{N}_e^\dagger \end{pmatrix}, \quad (47)$$

whose Majorana mass is given by M_{ee} . The four component lepton doublets are also given by,

$$\Psi_{L_\alpha} \equiv \begin{pmatrix} L_\alpha \\ 0 \end{pmatrix}, \quad (48)$$

which satisfy $P_L \Psi_{L_\alpha} = \Psi_{L_\alpha}$ with P_L being the projection operator on left-handed fermions.

In terms of them, the Lagrangian in Eq. (2) is rewritten as,

$$\mathcal{L}_\nu = \mathcal{L}_e + \mathcal{L}_{\mu\tau}, \quad (49)$$

$$\mathcal{L}_e = \frac{1}{2} \bar{\Psi}_e i \not{\partial} \Psi_e - \frac{M_{ee}}{2} \bar{\Psi}_e \Psi_e - (\lambda_e \bar{\Psi}_e \tilde{\Phi} P_L \Psi_{L_e} + \text{h.c.}), \quad (50)$$

$$\begin{aligned} \mathcal{L}_{\mu\tau} = & \bar{\Psi}_{\mu\tau} i \not{\partial} \Psi_{\mu\tau} - M_{\mu\tau} \bar{\Psi}_{\mu\tau} \Psi_{\mu\tau} - \left(\lambda_\mu \bar{\Psi}_{\mu\tau}^c \tilde{\Phi} P_L \Psi_{L_\mu} + \lambda_\tau \bar{\Psi}_{\mu\tau} \tilde{\Phi} P_L \Psi_{L_\tau} + \text{h.c.} \right) \\ & - \left(h_{e\mu} \sigma_1 \bar{\Psi}_e P_L \Psi_{\mu\tau} + h_{e\tau} \sigma_1^* \bar{\Psi}_e P_L \Psi_{\mu\tau}^c + \frac{1}{2} h_{\mu\mu} \sigma_2 \bar{\Psi}_{\mu\tau}^c P_L \Psi_{\mu\tau} + \frac{1}{2} h_{\tau\tau} \sigma_2^* \bar{\Psi}_{\mu\tau} P_L \Psi_{\mu\tau}^c + \text{h.c.} \right). \end{aligned} \quad (51)$$

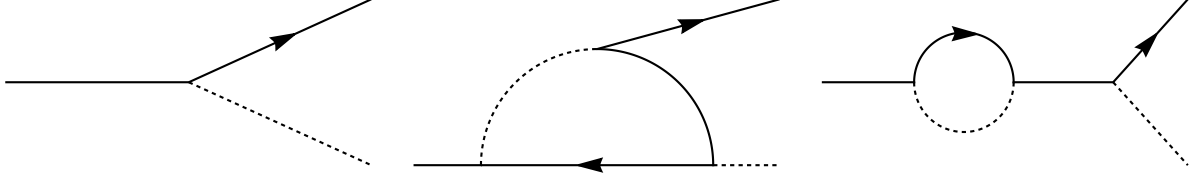


Figure 2. Tree, vertex, and wave-function diagrams for the decay of right-handed neutrinos. The plain solid lines, solid lines with arrows, and dashed lines correspond to the right-handed neutrinos, left-handed leptons, and scalar bosons, respectively.

Here, the bar over the fermion denotes the Dirac conjugate, the superscript c denotes the charge conjugation,⁸ and P_R is the projection operator on right-handed fermions. The usual lepton number⁹ is violated by the mass terms and Majorana Yukawa interactions in Eqs. (50) and (51).

As discussed in section III, both $M_{\mu\tau}$ and M_{ee} can be as large as $\mathcal{O}(10^7)$ GeV. Then, leptogenesis by the decay of the heavy right-handed neutrinos can be considered. Let us first focus on the decay of Ψ_e . In this case, the asymmetry is generated through the interference of the decay amplitudes given by

$$\mathcal{M}(\Psi_e \rightarrow \Psi_{L_e} + \Phi) = c_{e0} + c_{e1}\mathcal{F}_e, \quad (52)$$

$$\mathcal{M}(\Psi_e \rightarrow \Psi_{L_e}^c + \Phi^\dagger) = c_{e0}^* + c_{e1}^*\mathcal{F}_e. \quad (53)$$

Here, c_{e0} denotes the tree-level amplitude, c_{e1} is the one-loop amplitude where the kinematical loop-integration function \mathcal{F}_e is factored out. The tree-level and one-loop diagrams contributing to the decay are shown in Fig. 2. Note that Ψ_e does not decay into $\Psi_{L_{\mu,\tau}}^{(c)}$ at the tree level, and hence, we do not consider those modes. The lepton asymmetry is proportional to

$$|\mathcal{M}(\Psi_e \rightarrow \Psi_{L_e} + \Phi)|^2 - |\mathcal{M}(\Psi_e \rightarrow \Psi_{L_e}^c + \Phi^\dagger)|^2 = -4\text{Im}[c_{e0}c_{e1}^*]\text{Im}[\mathcal{F}_e]. \quad (54)$$

⁸ We define $\Psi^c \equiv -i\gamma^2\Psi^*$ and $\overline{\Psi}^c \equiv \overline{\Psi}^c$.

⁹ The usual lepton number corresponds to the phase rotations, $\Psi_{L_\alpha} \rightarrow e^{i\varphi}\Psi_{L_\alpha}$, $\Psi_e \rightarrow e^{i\varphi\gamma_5}\Psi_e$, and $\Psi_{\mu\tau} \rightarrow e^{i\varphi\gamma_5}\Psi_{\mu\tau}$, with $\varphi \in [0, 2\pi)$.

The imaginary part of \mathcal{F}_e appears from the on-shell singularities, while the imaginary part of $c_{e0}c_{e1}^*$ depends on the interaction coefficients appearing in the diagrams.

In the $U(1)_{L_\mu-L_\tau}$ symmetric phase, the flavor-changing ($\Psi_e \leftrightarrow \Psi_{\mu\tau}$) wave-function diagrams in Fig. 2 do not appear. Thus, such diagrams do not contribute to the asymmetry. The processes through the vertex diagrams with Majorana Yukawa coupling do not result in the pairs of $\Psi_{L_\alpha}^{(c)} + \Phi^{(\dagger)}$ in the symmetric phase. Thus, we look at the vertex diagrams with only Dirac Yukawa couplings. However, since the Dirac Yukawa couplings are flavor diagonal, we find,

$$c_{e0} \propto \lambda_e^* , \quad c_{e1} \propto \lambda_e^* |\lambda_e|^2 , \quad (55)$$

and hence, $\text{Im}[c_{e0}c_{e1}^*] = 0$. Therefore, no asymmetry is generated by the decay of Ψ_e in the $U(1)_{L_\mu-L_\tau}$ symmetric phase.

Next, we focus on the decay of $\Psi_{\mu\tau}$. The asymmetries are obtained from the following amplitudes,

$$\mathcal{M}(\Psi_{\mu\tau} \rightarrow \Psi_{L_\mu}^c + \Phi^\dagger) = c_{\mu0} + c_{\mu1}\mathcal{F}_\mu , \quad (56)$$

$$\mathcal{M}(\Psi_{\mu\tau} \rightarrow \Psi_{L_\tau} + \Phi) = c_{\tau0} + c_{\tau1}\mathcal{F}_\tau , \quad (57)$$

$$\mathcal{M}(\Psi_{\mu\tau}^c \rightarrow \Psi_{L_\mu} + \Phi) = c_{\mu0}^* + c_{\mu1}^*\mathcal{F}_\mu , \quad (58)$$

$$\mathcal{M}(\Psi_{\mu\tau}^c \rightarrow \Psi_{L_\tau}^c + \Phi^\dagger) = c_{\tau0}^* + c_{\tau1}^*\mathcal{F}_\tau . \quad (59)$$

Here, $c_{\mu0}$ and $c_{\tau0}$ are tree-level amplitudes, and $c_{\mu1}$ and $c_{\tau1}$ are one-loop amplitudes where the loop-integration functions $\mathcal{F}_{\mu,\tau}$ are factored out. In this case, the lepton asymmetry is proportional to the sum of,

$$|\mathcal{M}(\Psi_{\mu\tau}^c \rightarrow \Psi_{L_\mu} + \Phi)|^2 - |\mathcal{M}(\Psi_{\mu\tau} \rightarrow \Psi_{L_\mu}^c + \Phi^\dagger)|^2 = -4\text{Im}[c_{\mu0}^*c_{\mu1}]\text{Im}[\mathcal{F}_\mu] , \quad (60)$$

$$|\mathcal{M}(\Psi_{\mu\tau} \rightarrow \Psi_{L_\tau} + \Phi)|^2 - |\mathcal{M}(\Psi_{\mu\tau}^c \rightarrow \Psi_{L_\tau}^c + \Phi^\dagger)|^2 = -4\text{Im}[c_{\tau0}c_{\tau1}^*]\text{Im}[\mathcal{F}_\tau] . \quad (61)$$

As in the case of the decay of Ψ_e , we look at the vertex diagrams with only Dirac Yukawa

couplings, and we find

$$c_{\mu 0} \propto \lambda_\mu, \quad c_{\mu 1} \propto \lambda_\mu |\lambda_\tau|^2, \quad (62)$$

$$c_{\tau 0} \propto \lambda_\tau^*, \quad c_{\tau 1} \propto \lambda_\tau^* |\lambda_\mu|^2. \quad (63)$$

Note that, in the one-loop vertex diagrams of the decay mode into $\Psi_{L\mu}$, only $\Psi_{L\tau}^c$ appears as a virtual state, and vice versa. From Eqs. (62) and (63), we find that the decay of $\Psi_{\mu\tau}$ does not generate the lepton asymmetry. As a result, the decay of right-handed neutrinos in the $U(1)_{L\mu-L\tau}$ symmetric phase does not generate the lepton asymmetry. This consequence coincides with that in previous work [66].¹⁰

For $M_{\mu\tau}$ and $M_{ee} = \mathcal{O}(10)$ GeV leptogenesis via right-handed neutrino oscillations can be considered [67, 68]. In the $U(1)_{L\mu-L\tau}$ symmetric phase, however, the right-handed neutrinos have different $U(1)_{L\mu-L\tau}$ charges, and hence, the oscillations among them do not occur. Thus, leptogenesis via right-handed neutrino oscillations cannot work.

B. Leptogenesis in the $U(1)_{L\mu-L\tau}$ broken phase

Below let us discuss leptogenesis in the $U(1)_{L\mu-L\tau}$ broken phase. As we have seen in Sec. IV B, the $U(1)_{L\mu-L\tau}$ symmetry can be broken by the thermal effects for $\lambda_{\Phi\sigma} < 0$ with $|\lambda_{\Phi\sigma}| \gg \lambda_\sigma, g_{Z'}^2$. Hereafter, we assume that both σ_1 and σ_2 obtain non-vanishing expectation values in the early universe. In the broken phase, $U(1)_{L\mu-L\tau}$ charge is no longer conserved, and hence, leptogenesis by the right-handed neutrinos may take place. To discuss leptogenesis in the broken phase, we take the Majorana mass eigenstates of the right-handed neutrinos Ψ'_I ($I = 1, 2, 3$) with the mass eigenvalues M_I (see Eqs. (C3) and (C14)). Due to the nonzero $\langle\sigma_{1,2}\rangle$, one degree of freedom in $\sigma_{1,2}$ is absorbed into the gauge boson Z' , and the rest remains as physical degrees of freedom, S_1, S_2 , and P (see the Appendix A).

As the simplest possibility, let us discuss the non-thermal leptogenesis where the inflaton mainly decays into the right-handed neutrinos [48, 49]. The lepton asymmetry is gener-

¹⁰ In the reference, thermal leptogenesis has been argued with Dirac Yukawa couplings and Majorana masses for right-handed neutrinos under the exact $L_\mu - L_\tau$ symmetry.

ated by the subsequent decay of the right-handed neutrinos into the SM leptons and the Higgs bosons. In this scenario, the reheating temperature after inflation is much lower than all three right-handed neutrino masses, $T_R \ll M_I$. This condition can be satisfied for $M_{ee}, M_{\mu\tau} \gg T_R$. Such large mass parameters are consistent with the observed neutrino oscillations in the cases in Secs. III B and III C.

We also assume that the decay rates of the right-handed neutrinos are much larger than that of the inflaton, *i.e.*, $\Gamma_{D,I} \gg \Gamma_{\text{inf}}$. In this case, since the Hubble expansion rate at the reheating is also much smaller than the decay rates of the right-handed neutrinos, we may approximate that $\langle \sigma_{1,2} \rangle \propto T$ is time-independent to discuss leptogenesis.

The yields of the right-handed neutrinos from the inflaton decay are given by

$$Y_I \equiv \frac{n_I}{s} \simeq \left(\frac{\rho_R}{s} \times \frac{n_{\text{inf}}}{\rho_{\text{inf}}} \right) \Big|_{T=T_R} \times f_I . \quad (64)$$

Here, s is the entropy density, $\rho_{R,\text{inf}}$ are the energy densities of the radiation and the inflaton, respectively, and $n_{\text{inf},I}$ are the number densities of the inflaton and each right-handed neutrino Ψ'_I . The parameter f_I is the number of the right-handed neutrinos expected at the decay of one inflaton. Here, we assume that at least one of f_I is of $\mathcal{O}(1)$. In the second equality, we have used $\rho_R \simeq \rho_{\text{inf}}$ at the reheating time. By noting $\rho_R/s \simeq T_R$, $n_{\text{inf}}/\rho_{\text{inf}} \simeq 1/m_{\text{inf}}$ with m_{inf} being the inflaton mass, the yields amount to

$$Y_I \simeq \frac{T_R}{m_{\text{inf}}} \times f_I . \quad (65)$$

As the right-handed neutrinos immediately decay after the production, the yield of the lepton asymmetry is given by

$$Y_L \equiv \frac{\Delta n_L}{s} = \sum_I \tilde{\epsilon}_I \times \frac{n_I}{s} = \frac{T_R}{m_{\text{inf}}} \sum_I \tilde{\epsilon}_I f_I , \quad (66)$$

where Δn_L is the difference between the number densities of $(L_\alpha, \bar{l}_{R\alpha}^\dagger)$ and $(L_\alpha^\dagger, \bar{l}_{R\alpha})$, and $\tilde{\epsilon}_I$

denotes the asymmetry parameters of each right-handed neutrino defined by

$$\tilde{\epsilon}_I = \sum_{\alpha} \frac{\Gamma(\Psi'_I \rightarrow \Psi_{L\alpha} + \tilde{\Phi}) - \Gamma(\Psi'_I \rightarrow \Psi_{L\alpha}^c + \tilde{\Phi}^\dagger)}{\Gamma_{D,I}} . \quad (67)$$

We decompose $\tilde{\epsilon}_I$ as

$$\begin{aligned} \tilde{\epsilon}_I &= \frac{\sum_{\alpha} [\Gamma(\Psi'_I \rightarrow \Psi_{L\alpha} + \tilde{\Phi}) - \Gamma(\Psi'_I \rightarrow \Psi_{L\alpha}^c + \tilde{\Phi}^\dagger)]}{\sum_{\alpha} [\Gamma(\Psi'_I \rightarrow \Psi_{L\alpha} + \tilde{\Phi}) + \Gamma(\Psi'_I \rightarrow \Psi_{L\alpha}^c + \tilde{\Phi}^\dagger)]} \times \frac{\sum_{\alpha} [\Gamma(\Psi'_I \rightarrow \Psi_{L\alpha} + \tilde{\Phi}) + \Gamma(\Psi'_I \rightarrow \Psi_{L\alpha}^c + \tilde{\Phi}^\dagger)]}{\Gamma_{D,I}} \\ &\equiv \epsilon_I \times \text{Br}(\Psi'_I \rightarrow \Psi_L^{(c)} + \tilde{\Phi}^{(\dagger)}) , \end{aligned} \quad (68)$$

where ϵ_I denotes the asymmetry parameters of each right-handed neutrino when Ψ'_I decays into $\Psi_L + \tilde{\Phi}$ and $\Psi_L^c + \tilde{\Phi}^\dagger$ with the branching ratio, $\text{Br}(\Psi'_I \rightarrow \Psi_L^{(c)} + \tilde{\Phi}^{(\dagger)})$. Here, we sum over the flavor of leptons for both ϵ_I and the branching ratio.

To evaluate the lepton asymmetry, we present the relevant interactions of the right-handed neutrinos in the mass basis. The couplings to Z' are given by the covariant derivative as

$$\mathcal{L}'_{\text{kin}} = \frac{1}{2} \bar{\Psi}'_I i \gamma^\mu (\partial_\mu \delta_{IJ} - i g_{Z'} \gamma^5 Z'_\mu Q'_{IJ}) \Psi'_J , \quad (69)$$

where Q'_{IJ} can be read from Eq. (C7). The Dirac Yukawa matrix, λ'_ν , is given by

$$\mathcal{L}'_{\text{DY}} = -\lambda'_{\nu\alpha I} \bar{\Psi}'_I \tilde{\Phi} P_L \Psi_{L\alpha} - \lambda'^*_{\nu\alpha I} \bar{\Psi}_{L\alpha} P_R \tilde{\Phi}^\dagger \Psi'_I . \quad (70)$$

The breaking scalars couple with the right-handed neutrinos through the Majorana Yukawa term as

$$\mathcal{L}'_{\text{MY}} = - \sum_{X=S_1, S_2, P} \bar{\Psi}'_I F_{IJ}^X X \Psi'_J \quad (71)$$

with

$$F_{IJ}^X \equiv \frac{1}{2\sqrt{2}} (f_{IJ}^X - i\gamma^5 g_{IJ}^X) , \quad (72)$$

for $X = S_1, S_2, P$. See the Appendix C for the explicit form of these couplings.

First, we evaluate the branching ratio, $\text{Br}(\Psi'_I \rightarrow \Psi_L^{(c)} + \tilde{\Phi}^{(\dagger)})$. In addition to the decay into the SM lepton and Higgs, the right-handed neutrino can also decay into another lighter right-handed neutrino and the breaking scalar: $\Psi'_I \rightarrow \Psi'_J + X$, or another lighter right-handed neutrino and the $U(1)_{L_\mu - L_\tau}$ gauge field: $\Psi'_I \rightarrow \Psi'_J + Z'$. Here, we neglect $1 \rightarrow 3$ decay processes because their rates will be subdominant in the total decay rate due to the phase space suppression. The tree decay rates of $\Psi'_I \rightarrow \Psi_L^{(c)} + \tilde{\Phi}^{(\dagger)}$, $\Psi'_I \rightarrow \Psi'_J + X$, and $\Psi'_I \rightarrow \Psi'_J + Z'$ are given by

$$\Gamma_I^{\Psi_L \Phi} = \frac{M_I}{8\pi} [\lambda_\nu^\dagger \lambda'_\nu]_{II} , \quad (73)$$

$$\Gamma_I^{\Psi'_J X} = \frac{M_I}{128\pi} (1 - r_J^2) [(1 + r_J)^2 (f_{IJ}^X)^2 + (1 - r_J)^2 (g_{IJ}^X)^2] \Theta(M_I - M_J) , \quad (74)$$

$$\Gamma_I^{\Psi'_J Z'} = \frac{g_{Z'}^2 M_I (1 - r_J^2)^3}{64\pi r_{Z'}^2} |Q'_{IJ}|^2 \Theta(M_I - M_J) , \quad (75)$$

where $r_J \equiv M_J/M_I$, $r_{Z'} \equiv m_{Z'}/M_I$. Since $T_R \ll M_I$, $m_{Z'}$ and m_X evaluated at T_R satisfy $r_{Z'} \ll 1$ and $m_X/M_I \ll 1$ and we used these limits. From these decay rates, we obtain the branching ratio as

$$\text{Br}(\Psi'_I \rightarrow \Psi_L^{(c)} + \tilde{\Phi}^{(\dagger)}) \simeq \frac{\Gamma_I^{\Psi_L \Phi}}{\Gamma_{\text{tree}, I}} \equiv \frac{\Gamma_I^{\Psi_L \Phi}}{\Gamma_I^{\Psi_L \Phi} + \sum_{J, X} \Gamma_I^{\Psi'_J X} + \sum_J \Gamma_I^{\Psi'_J Z'}} , \quad (76)$$

where $\Gamma_{\text{tree}, I}$ is the sum of Eqs. (73), (74), and (75). Here, we used $\Gamma_{D, I} \simeq \Gamma_{\text{tree}, I}$. Note that $\text{Br}(\Psi'_I \rightarrow \Psi_L^{(c)} + \tilde{\Phi}^{(\dagger)}) = 1$ for the lightest right-handed neutrino, $I = 1$.

Next, we evaluate ϵ_I . To this end, we consider the tree and one-loop diagrams of the decay of the right-handed neutrinos into $\Psi_L^{(c)} + \tilde{\Phi}^{(\dagger)}$. In our setup, three types of one-loop diagrams contribute to the asymmetry parameters. In Fig. 3, we show the relevant diagrams:

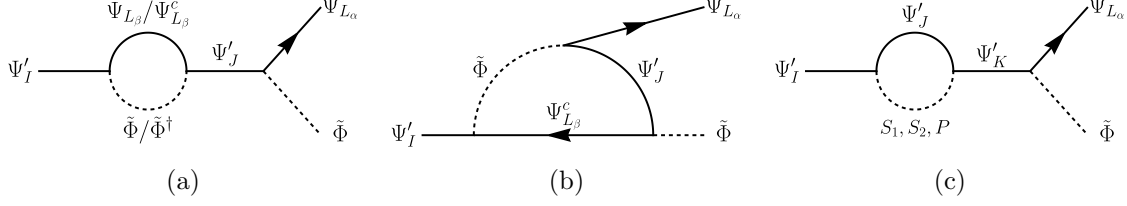


Figure 3. One-loop diagrams for decays of right-handed neutrinos.

(a) wave-function ($\Psi_L \Phi$ loop), (b) vertex ($\Psi_L \Phi \Psi'$ loop), and (c) wave-function ($\Psi' X$ loop). The contributions from other diagrams are negligible as discussed in the Appendix D. Thus, ϵ_I is given by the sum of asymmetry parameters from the three diagrams as

$$\epsilon_I = \epsilon_I^{(a)} + \epsilon_I^{(b)} + \epsilon_I^{(c)} , \quad (77)$$

where

$$\epsilon_I^{(a)} = -\frac{1}{8\pi} \sum_J \frac{M_I M_J}{M_I^2 - M_J^2} \frac{(M_I^2 - M_J^2)^2}{(M_I^2 - M_J^2)^2 + M_I^2 \Gamma_{\text{tree},J}^2} \frac{\text{Im}[[\lambda_\nu^\dagger \lambda'_\nu]_{IJ}^2]}{[\lambda_\nu^\dagger \lambda'_\nu]_{II}} , \quad (78)$$

$$\epsilon_I^{(b)} = -\frac{1}{8\pi} \sum_J \frac{\text{Im}[[\lambda_\nu^\dagger \lambda'_\nu]_{IJ}^2]}{[\lambda_\nu^\dagger \lambda'_\nu]_{II}} r_J \left[1 - (1 + r_J^2) \log \left(\frac{1 + r_J^2}{r_J^2} \right) \right] , \quad (79)$$

$$\begin{aligned} \epsilon_I^{(c)} = & \sum_{J,K} \frac{1 - r_J^2}{128\pi(1 - r_K^2)[\lambda_\nu^\dagger \lambda'_\nu]_{II}} \frac{(M_I^2 - M_K^2)^2}{(M_I^2 - M_K^2)^2 + M_I^2 \Gamma_{\text{tree},K}^2} \Theta(M_I - M_J) \\ & \times \sum_{X=S_1, S_2, P} \left[-(1 + r_K) \text{Im}[\lambda_\nu^\dagger \lambda'_\nu]_{IJ} \{ (1 + r_J)^2 f_{IJ}^X f_{JK}^X + (1 - r_J)^2 g_{IJ}^X g_{JK}^X \} \right. \\ & \left. + (1 - r_K) \text{Re}[\lambda_\nu^\dagger \lambda'_\nu]_{IJ} \{ (1 + r_J)^2 f_{IJ}^X g_{JK}^X - (1 - r_J)^2 g_{IJ}^X f_{JK}^X \} \right] . \quad (80) \end{aligned}$$

The fractions with $\Gamma_{\text{tree},J}^2$ and $\Gamma_{\text{tree},K}^2$ come from the finite width of the right-handed neutrinos and regulates the asymmetry parameters in the resonant limit, $M_I \rightarrow M_{J,K}$ [69].

From these formulae, we evaluate the asymmetry parameters in the normal and inverted ordering of active neutrino masses assuming the parameters obtained in Secs. III B and III C. The results are summarized in Tab. II. Here, we fix the expectation values of $\sigma_{1,2}$ in the

Table II. Asymmetry parameters in our setup.

		Diagrams			Total ϵ
		(a)	(b)	(c)	
Normal Ordering	ϵ_1	7×10^{-8}	3×10^{-8}	0	1×10^{-7}
	ϵ_2	5×10^{-7}	-4×10^{-7}	-5×10^{-6}	-5×10^{-6}
	ϵ_3	-5×10^{-7}	4×10^{-7}	-5×10^{-6}	-5×10^{-6}
Inverted Ordering	ϵ_1	-5×10^{-8}	-2×10^{-8}	0	-6×10^{-8}
	ϵ_2	-8×10^{-8}	7×10^{-8}	3×10^{-6}	3×10^{-6}
	ϵ_3	6×10^{-8}	-7×10^{-8}	3×10^{-6}	3×10^{-6}

vacuum and at the reheating for both the orderings as

$$\langle \sigma_1 \rangle_0 = 80 \text{ GeV} , \quad \langle \sigma_2 \rangle_0 = 50 \text{ GeV} , \quad \langle \sigma_{1,2} \rangle_{T_R} = 10^5 \text{ GeV} , \quad (81)$$

which can be realized by

$$\lambda_{\sigma_1} = \lambda_{\sigma_2} = 3 \times 10^{-4} , \quad \lambda_{\Phi \sigma_1} = \lambda_{\Phi \sigma_2} = -3 \times 10^{-3} , \quad T_R \simeq 3 \times 10^4 \text{ GeV} . \quad (82)$$

In the normal ordering case, we also fix the parameters as¹¹

$$|M_{ee}| = 5 \times 10^6 \text{ GeV} , \quad \lambda_\mu = 1 , \quad |h_{e\tau}| = 1 . \quad (83)$$

In this case, the mass eigenvalues of the right-handed neutrinos become

$$\begin{aligned} M_1 &\simeq 5.0 \times 10^6 \text{ GeV} , \quad M_2 \simeq M_3 \simeq 1.4 \times 10^7 \text{ GeV} , \\ M_3 - M_2 &\simeq 1.2 \times 10^3 \text{ GeV} . \end{aligned} \quad (84)$$

Here, M_2 and M_3 are highly degenerate because they are dominated by $M_{\mu\tau}$ and their

¹¹ Here, we consider a large value of $h_{e\mu}$, whose effect was not discussed in the previous section. Since we investigate non-thermal leptogenesis, the right-handed neutrinos are not in the thermal bath. They decay promptly after being generated from the inflatons, and hence we expect that they do not alter the potential of σ . Even if finite density effects of the right-handed neutrinos exist, such effects are negligible because their number density is much smaller than that of other particles in the thermal bath.

degeneracy is slightly broken by $h_{\tau\tau}\langle\sigma_2\rangle_{T_R}$, which is much smaller than $M_{\mu\tau}$.

On the other hand, in the inverted ordering case, we fix

$$|M_{ee}| = 5 \times 10^6 \text{ GeV} , \quad \lambda_\tau = 1 , \quad |h_{e\mu}| = 1 , \quad (85)$$

which leads to

$$\begin{aligned} M_1 &\simeq 5.0 \times 10^6 \text{ GeV} , \quad M_2 \simeq M_3 \simeq 1.4 \times 10^7 \text{ GeV} , \\ M_3 - M_2 &\simeq 5.2 \times 10^2 \text{ GeV} , \end{aligned} \quad (86)$$

where M_2 and M_3 are highly degenerate as in the normal ordering case.

Finally, we evaluate the resultant yield of the lepton asymmetry. Since the observed baryon asymmetry is $n_B/s \simeq 8.7 \times 10^{-11}$ [58] and the sphaleron processes convert the lepton asymmetry generated at high temperatures into baryon asymmetry as $n_B \simeq (28/79) \times n_{B-L}$, the success of leptogenesis requires $Y_L \simeq -2.5 \times 10^{-10}$.

We first consider the case where the inflaton mainly decays into Ψ'_1 . In this case, we adopt $f_1 = 2$ and $f_2 = f_3 = 0$ as a typical value when the inflaton decays into a pair of the right-handed neutrinos. From Eq. (66), the lepton asymmetry becomes

$$Y_L \simeq \frac{2T_R}{m_{\text{inf}}} \epsilon_1 . \quad (87)$$

Since the decay of the inflaton into a pair of Ψ'_1 requires $m_{\text{inf}} > 2M_1$, we obtain the maximum lepton asymmetry as

$$Y_L \lesssim \frac{T_R}{M_1} \epsilon_1 \simeq \begin{cases} 6 \times 10^{-10} & (\text{Normal Ordering}) \\ -4 \times 10^{-10} & (\text{Inverted Ordering}) \end{cases} . \quad (88)$$

This value in the inverted ordering is compatible with the observed baryon asymmetry in the universe. As we will see below, the washout effects reduce Y_L by a factor of a few at most.

Next, we consider the case where the inflaton mainly decays into Ψ'_2 and Ψ'_3 . As a typical value, we adopt $f_2 = f_3 = 1$. While $\Psi'_{2,3}$ mainly decays into the left-handed lepton and Higgs, a part of them generates Ψ'_1 . Thus, even if the inflaton does not directly decay into Ψ'_1 , f_1 is effectively nonzero and estimated as¹²

$$f_1 = \sum_{I=2,3} f_I \left[1 - \text{Br}(\Psi'_I \rightarrow \Psi_L^{(c)} + \tilde{\Phi}^{(\dagger)}) \right] \simeq 0.22, \quad (89)$$

for both the normal and inverted orderings. From $m_{\text{inf}} \gtrsim 2M_3$, we obtain the maximum lepton asymmetry as

$$Y_L \lesssim \frac{T_R}{2M_3} \sum_I \tilde{\epsilon}_I f_I \simeq \begin{cases} -1 \times 10^{-8} & (\text{Normal Ordering}) \\ 6 \times 10^{-9} & (\text{Inverted Ordering}) \end{cases}. \quad (90)$$

This value in the normal ordering is compatible with the observed baryon asymmetry of the universe.

Note that the signs of asymmetry parameters of leptogenesis above are reversed when we adopt the CP phases opposite to those in Secs. III B and III C. However, such values of the Dirac phase δ ($\sim 90^\circ$) are disfavored in the current neutrino oscillation experiments.

C. Wash-out effects in non-thermal leptogenesis

In the presence of lepton number violating processes, lepton asymmetry in the thermal bath is washed out due to the unbalance between the rates of the processes including leptons and anti-leptons. We evaluate the wash-out effects from the inverse decay of Ψ'_I and lepton number violating scatterings with $\Delta L = 1$ and 2 in our scenario. It turns out that the effects are not significant with $T_R \lesssim 4 \times 10^4 \text{ GeV}$ in the case of the benchmark point in the previous subsection.

¹² The branching ratio of Ψ'_3 into Ψ'_2 is negligible due to the degeneracy of the masses.

1. Inverse decay

The inverse decay of Ψ'_I from the thermal bath violates lepton number by $\Delta L = 1$. Since non-thermal leptogenesis requires $M_I \gg T_R$, the inverse decay rate is suppressed. We here estimate the condition of $z_I \equiv M_I/T_R$ for the wash-out effect of the inverse decay to be inefficient. The inverse decay rate, $\Gamma_{\text{ID},I}$, is given by

$$\begin{aligned}\Gamma_{\text{ID},I} &= \Gamma_I^{\Psi_L \Phi} \times \frac{n_I^{\text{eq}}}{n^{\text{eq}}}, \\ n_I^{\text{eq}} &= g_N \left(\frac{M_I T}{2\pi} \right)^{3/2} e^{-\frac{M_I}{T}}, \\ n^{\text{eq}} &= \frac{3}{4} \frac{\zeta(3)}{\pi^2} T^3,\end{aligned}\tag{91}$$

where $g_N = 2$.¹³ From the above equations, $\Gamma_{\text{ID},I}$ is obtained with respect to z_I as

$$\Gamma_{\text{ID},I}(z_I) \simeq \frac{1}{8\pi} \sum_{\alpha} |\lambda'_{\alpha I}|^2 M_I z_I^{3/2} e^{-z_I},\tag{92}$$

and

$$\frac{\Gamma_{\text{ID},I}(z_I)}{H(T_R)} \simeq 8 \times 10^9 \sum_{\alpha} |\lambda'_{\alpha I}|^2 \left(\frac{5 \times 10^6 \text{ GeV}}{M_I} \right) z_I^{7/2} e^{-z_I}.\tag{93}$$

From $\sum_{\alpha} |\lambda'_{\alpha I}|^2 \sim 1$ in our setup, it suggests that $\Gamma_{\text{ID},I}(z_I)/H(T_R) < 1$ can be satisfied for all I 's if

$$T_R \lesssim 1.4 \times 10^5 \text{ GeV},\tag{94}$$

when $M_1 \simeq 5 \times 10^6 \text{ GeV}$ and $M_{2,3} \simeq 1.4 \times 10^7 \text{ GeV}$.

¹³ In the limit of $\Delta n_L/n^{\text{eq}} \ll 1$, the lepton asymmetry follows $\Delta \dot{n}_L + 3H\Delta n_L \supset -\Gamma_{\text{ID},I}\Delta n_L$.

2. $\Delta L = 1$ scatterings

Scattering processes of Ψ'_I and left-handed leptons with $\Delta L = 1$ also contribute to the wash-out effects, *e.g.*, $\Psi'_I + \Psi_{L_\alpha} \rightarrow f + \bar{f}$, where f is a SM fermion. Here, the right-handed neutrinos do not appear in the final state since $M_I \gg T_R$ in non-thermal leptogenesis. The Boltzmann equation of the lepton asymmetry in terms of Y_L is given by,

$$\dot{Y}_L \simeq \sum_I (\tilde{\epsilon}_I \Gamma_{D,I} Y_I - \Gamma_{\Delta L=1,I} Y_L Y_I) . \quad (95)$$

where the second term expresses the wash-out effect from the $\Delta L = 1$ scatterings. Here, Y_L is at most $\sum_I \tilde{\epsilon}_I Y_I(T_R) = \sum_I \tilde{\epsilon}_I f_I T_R / m_{\text{inf}}$. Assuming that the inflaton mainly decays into one of Ψ'_I with favorable $\tilde{\epsilon}_I$, it is sufficient to focus on such a Ψ'_I in the Boltzmann equation;

$$\dot{Y}_L \gtrsim \left(\Gamma_{D,I} - \Gamma_{\Delta L=1,I} f_I \frac{T_R}{m_{\text{inf}}} \right) \tilde{\epsilon}_I Y_I . \quad (96)$$

This shows that the wash-out effect due to the $\Delta L = 1$ scattering becomes negligible when $\Gamma_{D,I} \gg \Gamma_{\Delta L=1,I}$ because $T_R / m_{\text{inf}} \ll 1$ and $f_I = \mathcal{O}(1)$. Actually, for $T \ll M_I$, $\Gamma_{D,I} \gg \Gamma_{\Delta L=1,I}$ is satisfied for Ψ'_I 's interacting with the SM thermal bath as seen in, for example, Fig. 5 of Ref. [70]. We have also checked that $\Gamma_{D,I} \gg \Gamma_{\Delta L=1,I}$ is satisfied when we consider interactions involving the $U(1)_{L_\mu - L_\tau}$ sector particles.

3. $\Delta L = 2$ scatterings

Finally, scattering processes between left-handed leptons and SM Higgs with a virtual Ψ'_I can violate the lepton number by $\Delta L = 2$ like $\Psi_{L_\alpha} \Phi \rightarrow \Psi_{L_\beta}^c \Phi^\dagger$ and $\Psi_{L_\alpha} \Psi_{L_\beta} \rightarrow \Phi \Phi$.

For $T \ll M_I$, the invariant amplitude squared is given by

$$|\mathcal{M}_{\Delta L=2}|^2 \simeq \sum_I N_d |\lambda'_{\beta I} M_I^{-1} \lambda'_{\alpha I}|^2 (p_{L_\alpha} \cdot p_{L_\beta}) = N_d |\lambda_\beta [M_{R,\text{eff}}^{-1}]_{\beta\alpha} \lambda_\alpha|^2 (p_{L_\alpha} \cdot p_{L_\beta}), \quad (97)$$

where $N_d = 10$ is a numerical coefficient from relevant diagrams ($N_d = 8$ comes from

$\Psi_{L_\alpha}\Phi \rightarrow \Psi_{L_\beta}^c\Phi^\dagger$ and $N_d = 2$ comes from $\Psi_{L_\alpha}\Psi_{L_\beta} \rightarrow \Phi\Phi$), and p_{L_α} is the four-momentum of left-handed lepton with α flavor. We used the relations of Yukawa couplings and masses between the flavor and mass bases in the last equality (see Appendix C). From this amplitude squared, the cross-section of the $\Delta L = 2$ scatterings is obtained as

$$[\sigma v]_{\beta\alpha} \sim \frac{N_d}{32\pi} |\lambda_\beta [M_{R,\text{eff}}^{-1}]_{\beta\alpha} \lambda_\alpha|^2, \quad (98)$$

where, as a typical value, we took the energies of SM particles as T .

For the neutrino oscillation parameters discussed in Sec. III B for the normal ordering, $h_{\mu\mu} = h_{e\mu} = 0$, which leads to

$$M_{R,\text{eff}}^{-1} = \begin{pmatrix} M_{ee}^{-1} & -\frac{h_{e\tau}\langle\sigma_1\rangle}{M_{ee}M_{\mu\tau}} & 0 \\ -\frac{h_{e\tau}\langle\sigma_1\rangle}{M_{ee}} & -\frac{h_{e\tau}^2\langle\sigma_1\rangle^2 + h_{\tau\tau}M_{ee}\langle\sigma_2\rangle}{M_{ee}M_{\mu\tau}^2} & M_{\mu\tau}^{-1} \\ 0 & M_{\mu\tau}^{-1} & 0 \end{pmatrix}. \quad (99)$$

For the benchmark point of non-thermal leptogenesis discussed in Sec. V B,

$$\begin{aligned} \lambda_e &\sim 10^{-4}, \quad \lambda_\mu \sim 1, \quad \lambda_\tau \sim 10^{-8}, \quad h_{e\tau} \sim 1, \quad h_{\tau\tau} \sim 10^{-3}, \\ M_{ee} &\sim 5 \times 10^6 \text{ GeV}, \quad M_{\mu\tau} \sim 10^7 \text{ GeV}, \quad \langle\sigma_i\rangle \sim T_R \sim 10^5 \text{ GeV}, \end{aligned} \quad (100)$$

the largest wash-out effect is for $\alpha = \beta = \mu$, and the scattering rate is given by

$$\Gamma_{\Delta L=2}|_{\mu\mu} \equiv [\sigma v]_{\mu\mu} n^{\text{eq}} \simeq \frac{N_d \zeta(3)}{32\pi^3} |\lambda_\mu|^4 |[M_{R,\text{eff}}^{-1}]_{\mu\mu}|^2 T^3. \quad (101)$$

Then, $\Gamma_{\Delta L=2}|_{\mu\mu} < H$ requires

$$T_R \lesssim 4 \times 10^4 \text{ GeV}. \quad (102)$$

Since T_R in our benchmark point is close to this bound, the generated lepton asymmetry estimated in the previous subsection may be reduced by about a factor of two. Therefore,

the result for inverted ordering in Eq.(88) is barely consistent with the observed baryon asymmetry.¹⁴ On the other hand, that for normal ordering in Eq.(90) is sufficiently large to explain the observed value.

VI. CONCLUSION AND DISCUSSION

An extension of the SM with the gauged $U(1)_{L_\mu-L_\tau}$ symmetry can explain the muon $g-2$ anomaly. The gauged $U(1)_{L_\mu-L_\tau}$ symmetry is also consistent with the observed neutrino oscillations through the seesaw mechanism where three right-handed neutrinos $\bar{N}_e, \bar{N}_\mu, \bar{N}_\tau$ have the $U(1)_{L_\mu-L_\tau}$ charges 0, -1 , $+1$, respectively. In this paper, we investigated if leptogenesis can work while explaining the neutrino masses and muon $g-2$ anomaly at the same time.¹⁵

In our discussion, we sought the scenario where all the right-handed neutrinos are much heavier than the electroweak scale. Such a spectrum is highly non-trivial because right-handed neutrino masses are typically tied to the $U(1)_{L_\mu-L_\tau}$ breaking scale, 10–100 GeV. Nevertheless, we found that it is possible that all the right-handed neutrinos can be as heavy as 10^7 GeV only when the Yukawa couplings have specific structures as in Eqs.(16) and (26).

We also found that leptogenesis requires $U(1)_{L_\mu-L_\tau}$ symmetry breaking in the early universe because the $U(1)_{L_\mu-L_\tau}$ symmetry prohibits the flavor mixing among the right-handed neutrinos. As we have seen, however, the gauge and self interactions of the breaking fields σ 's tend to restore the $U(1)_{L_\mu-L_\tau}$ symmetry. Thus, to achieve the $U(1)_{L_\mu-L_\tau}$ broken phase in the early universe, we assumed a sizable negative value of Higgs- σ coupling $\lambda_{\Phi\sigma}$, which leads to $\langle\sigma\rangle \sim \sqrt{|\lambda_{\Phi\sigma}|/\lambda_\sigma} T$.

With these observations, we considered non-thermal leptogenesis and estimated the generated lepton asymmetry for both orderings of active neutrino masses. Even taking into account the wash-out effects on the asymmetry, we found the parameter points to gener-

¹⁴ In our analysis, we have not sought the optimal value of the lepton asymmetry for each ordering, and it is possible to achieve a larger lepton asymmetry by a factor of $\mathcal{O}(1)$.

¹⁵ In Ref.[71], leptogenesis has been discussed in a setup where the Z' mass and the $U(1)_{L_\mu-L_\tau}$ breaking scale are highly separated by considering a hierarchical charge assignment between the $U(1)_{L_\mu-L_\tau}$ breaking fields and the SM leptons.

ate a sufficient lepton asymmetry compatible with the observed baryon asymmetry of the universe. Therefore, we conclude that this model can explain the above three phenomena beyond the SM simultaneously.

In closing, we should mention that this scenario will be tested from various aspects in near future. Firstly, the extra neutral gauge boson Z' explaining the muon $g - 2$ anomaly will be probed by COHERENT [72] and NA64 μ at CERN [73, 74]. Secondly, improvement of the upper bound on the sum of active neutrino masses from the CMB observations will probe this scenario. To have the right-handed neutrino masses much larger than $\langle\sigma_{1,2}\rangle_0$, our scenario requires $\sum m_i \gtrsim 0.18\text{eV}$, which will be robustly tested in the future CMB observations such as CMB-S4 [75]. Finally, theoretical and experimental progress on the $0\nu\beta\beta$ decay will also be important for its test because relatively large values of the effective neutrino mass are suggested for this successful non-thermal leptogenesis as Eqs. (23) and (29).

ACKNOWLEDGMENTS

The authors thank K. Asai and T. Shimomura for useful communications. The authors also thank S. Kobayashi for his useful Feynman diagram drawer. This work was supported by JSPS KAKENHI Grant Nos. 18H05542, 21H04471, 22K03615 (M.I.), and 20J20248 (K.M.). K.M. was supported by the Program of Excellence in Photon Science.

Appendix A: Symmetry breaking sector

In this appendix, we summarize the symmetry breaking sector of the $U(1)_{L_\mu-L_\tau}$ model. In our scenario, we considered two SM singlet scalar bosons, $\sigma_{1,2}$, with the $U(1)_{L_\mu-L_\tau}$ charge +1 and +2, respectively.

1. Model with a single scalar

For the sake of brevity, let us first consider the model with a single scalar, σ . The scalar potential of σ and the Higgs doublet Φ is given by,

$$V(\Phi, \sigma) = -\mu_\sigma^2 |\sigma|^2 - \mu_\Phi^2 \Phi^\dagger \Phi + \lambda_\sigma |\sigma|^4 + \lambda_\Phi (\Phi^\dagger \Phi)^2 + \lambda_{\Phi\sigma} |\sigma|^2 (\Phi^\dagger \Phi) , \quad (\text{A1})$$

where μ_σ^2, μ_Φ^2 express mass parameters for each scalar field, $\lambda_\sigma, \lambda_\Phi$ are quartic self-couplings, and $\lambda_{\Phi\sigma}$ is a Higgs- σ coupling. As we have discussed in Sec. IV B, we assume $\lambda_{\Phi\sigma} < 0$, while λ_σ and λ_Φ are positive. Around the vacuum, we decompose Φ and σ as,

$$\Phi = \begin{pmatrix} H^+ \\ v_{\text{EW}} + \frac{1}{\sqrt{2}}(\hat{H} + ia) \end{pmatrix} , \quad \sigma = v + \frac{1}{\sqrt{2}}(\hat{S} + iA) , \quad (\text{A2})$$

where v_{EW} and v are VEVs. The charged Higgs scalar H^+ and the CP-odd scalars a and A are would-be Goldstone modes, which are set to be zero in the unitary gauge.

From $\partial V / \partial \hat{H} = \partial V / \partial \hat{S} = 0$, we find

$$\mu_\Phi^2 = 2\lambda_\Phi v_{\text{EW}}^2 + \lambda_{\Phi\sigma} v^2 , \quad \mu_\sigma^2 = 2\lambda_\sigma v^2 + \lambda_{\Phi\sigma} v_{\text{EW}}^2 . \quad (\text{A3})$$

The squared masses of the CP-even scalars are given by,

$$M^2 = \begin{pmatrix} 4\lambda_\Phi v_{\text{EW}}^2 & 2\lambda_{\Phi\sigma} v_{\text{EW}} v \\ 2\lambda_{\Phi\sigma} v_{\text{EW}} v & 4\lambda_\sigma v^2 \end{pmatrix} , \quad (\text{A4})$$

in the (\hat{H}, \hat{S}) basis. The mass eigenstates are obtained by,

$$\begin{pmatrix} H \\ S \end{pmatrix} = \begin{pmatrix} \cos \theta & \sin \theta \\ -\sin \theta & \cos \theta \end{pmatrix} \begin{pmatrix} \hat{H} \\ \hat{S} \end{pmatrix} , \quad (\text{A5})$$

where

$$\tan 2\theta \simeq \frac{\lambda_{\Phi\sigma} v v_{\text{EW}}}{\lambda_{\Phi} v_{\text{EW}}^2 - \lambda_{\sigma} v^2} . \quad (\text{A6})$$

As we are interested in the parameter region where $\lambda_{\Phi} \gg |\lambda_{\Phi\sigma}|, \lambda_{\sigma}$ with $v \simeq 10 - 100 \text{ GeV}$, we approximate Eq. (A6) by,

$$\theta \simeq \frac{1}{2} \frac{\lambda_{\Phi\sigma} v v_{\text{EW}}}{\lambda_{\Phi} v_{\text{EW}}^2} \simeq \frac{2\lambda_{\Phi\sigma} v v_{\text{EW}}}{m_H^2} , \quad (\text{A7})$$

where the mass eigenvalues are given by,

$$m_H^2 = 4\lambda_{\Phi} v_{\text{EW}}^2 (1 + \mathcal{O}(\lambda_{\Phi\sigma}^2)) , \quad m_S^2 = 4\lambda_{\sigma} v^2 (1 + \mathcal{O}(\lambda_{\Phi\sigma}^2)) . \quad (\text{A8})$$

To reproduce the observed Higgs mass $m_H \simeq 125 \text{ GeV}$ and $v_{\text{EW}} \simeq 174 \text{ GeV}$, we take $\lambda_{\Phi} \simeq 0.13$.

To the leading order of $\lambda_{\Phi\sigma}$ and λ_{σ} , the scalar couplings relevant to H and S decays are given by,

$$\mathcal{L} \supset -\frac{1}{2} g_{HSS} H S^2 - \frac{1}{2} g_{HAA} H A^2 - \frac{1}{2} g_{SAA} S A^2 , \quad (\text{A9})$$

with

$$g_{HSS} \simeq \frac{1}{\sqrt{2}} \frac{m_H^2}{v} \times \theta , \quad g_{HAA} \simeq \frac{1}{\sqrt{2}} \frac{m_H^2}{v} \times \theta , \quad g_{SAA} \simeq \frac{1}{\sqrt{2}} \frac{m_S^2}{v} . \quad (\text{A10})$$

Although the couplings to A are vanishing in the unitary gauge, they are useful to estimate the Higgs decay rate into Z' through the Goldstone equivalence theorem. The scalar couplings to Z' in the unitary gauge are also obtained from the kinetic term, $|D_{\mu}\sigma|^2$, as

$$\mathcal{L} \supset \frac{1}{2} \frac{\sqrt{2} m_{Z'}^2}{v} (S - \theta H) Z'_{\mu} Z'^{\mu} , \quad (\text{A11})$$

where

$$m_{Z'}^2 = 2g_{Z'}^2 Q_\sigma^2 v^2 , \quad (\text{A12})$$

with Q_σ being the $U(1)_{L_\mu-L_\tau}$ charge of σ .

Now, let us calculate the decay rates of H and S . The decay rates into a pair of Z' 's are given by,

$$\Gamma_{H \rightarrow Z' Z'} = \frac{1}{16\pi} \frac{M_Z'^4}{v^2 m_H} \theta^2 \left(2 + \frac{m_H^4}{4m_{Z'}^4} \left(1 - \frac{2m_{Z'}^2}{m_H^2} \right)^2 \right) \simeq \frac{1}{64\pi} \frac{m_H^3}{v^2} \theta^2 , \quad (\text{A13})$$

$$\Gamma_{S \rightarrow Z' Z'} = \frac{1}{16\pi} \frac{M_Z'^4}{v^2 m_S} \left(2 + \frac{m_S^4}{4m_{Z'}^4} \left(1 - \frac{2m_{Z'}^2}{m_S^2} \right)^2 \right) \simeq \frac{1}{64\pi} \frac{m_S^3}{v^2} . \quad (\text{A14})$$

These decay rates are in agreement with those into the Goldstone modes, $\Gamma_{H \rightarrow AA}$ and $\Gamma_{S \rightarrow AA}$, which demonstrates the Goldstone equivalence theorem. The Higgs boson also decays into a pair of S 's with the decay rate

$$\Gamma_{H \rightarrow SS} = \frac{1}{32\pi} \frac{g_{HSS}^2}{m_H} \left(1 - \frac{4m_S^2}{m_H^2} \right)^{1/2} \simeq \frac{1}{64\pi} \frac{m_H^3}{v^2} \theta^2 , \quad (\text{A15})$$

where we have assumed $m_H \gg m_S$ in the second equality. In Fig. 4, we show the partial decay rates of S into a pair of Z' 's and those into the SM particles. The figure shows that S dominantly decays into Z' for $\sin \theta \ll 1$. As Z' mainly decays into a pair of ν 's, the decays of S are virtually invisible.

Since decays of S and Z' are invisible, both $\Gamma_{H \rightarrow Z' Z'}$ and $\Gamma_{H \rightarrow SS}$ contribute to the invisible decay mode of the Higgs boson as

$$\text{Br}(H \rightarrow \text{invisible}) = \frac{\Gamma_{H \rightarrow Z' Z'} + \Gamma_{H \rightarrow SS}}{\Gamma_{\text{SM}} + \Gamma_{H \rightarrow Z' Z'} + \Gamma_{H \rightarrow SS}} , \quad (\text{A16})$$

where Γ_{SM} is the predicted value of the Higgs decay width into the SM particles, $\Gamma_{\text{SM}} \simeq$

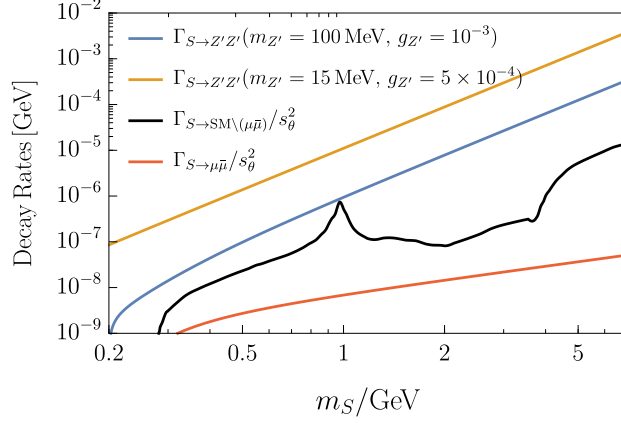


Figure 4. The decay rates of S . The black line shows the total decay rate into the SM particles other than $\mu\bar{\mu}$ while the red line shows that into $\mu\bar{\mu}$, which are extracted from Ref. [76]. They are normalized by the mixing angle $s_\theta^2 \equiv \sin^2 \theta$. The blue line shows the decay rate of S into a pair of Z' 's for $m_{Z'} = 100$ MeV and $g_{Z'} = 10^{-3}$ ($\langle\sigma\rangle_0 = 100$ GeV) for $\sin \theta \ll 1$. The yellow line shows the decay rate into a pair of Z' 's for $m_{Z'} = 15$ MeV and $g_{Z'} = 5 \times 10^{-4}$ ($\langle\sigma\rangle_0 = 30$ GeV) for $\sin \theta \ll 1$.

4.1 MeV [77]. For $m_H \gg m_{Z'}, m_S$, we obtain

$$\Gamma_{H \rightarrow Z'Z'} + \Gamma_{H \rightarrow SS} \simeq \frac{\lambda_{\Phi\sigma}^2 v_{\text{EW}}^2}{8\pi m_H}. \quad (\text{A17})$$

Thus, from the upper limit on the branching fraction of Higgs invisible decay mode, $\text{Br}(H \rightarrow \text{invisible}) < 0.11$ [64], we find the upper limit on $|\lambda_{\Phi\sigma}|$,

$$|\lambda_{\Phi\sigma}| \simeq \left(\frac{8\pi m_H \Gamma_{\text{SM}}}{v_{\text{EW}}^2} \times \text{Br}(H \rightarrow \text{invisible}) \right)^{1/2} \lesssim 7 \times 10^{-3}. \quad (\text{A18})$$

2. Model with two scalars

Next, let us summarize the scalar sector with two $U(1)_{L_\mu-L_\tau}$ charged fields σ_1 and σ_2 . In this case, the scalar potential is extended to,

$$\begin{aligned}
V(\Phi, \sigma_1, \sigma_2) = & -\mu_\Phi^2 \Phi^\dagger \Phi - \mu_{\sigma_1}^2 |\sigma_1|^2 - \mu_{\sigma_2}^2 |\sigma_2|^2 \\
& + \lambda_\Phi (\Phi^\dagger \Phi)^2 + \lambda_{\sigma_1} |\sigma_1|^4 + \lambda_{\sigma_2} |\sigma_2|^4 \\
& + \lambda_{\Phi\sigma_1} (\Phi^\dagger \Phi) |\sigma_1|^2 + \lambda_{\Phi\sigma_2} (\Phi^\dagger \Phi) |\sigma_2|^2 \\
& - c\sigma_2^* \sigma_1^2 - c\sigma_2 \sigma_1^{*2} ,
\end{aligned} \tag{A19}$$

where c is a real-valued coupling constant with mass dimension one. We have omitted a possible $|\sigma_1|^2 |\sigma_2|^2$ term for simplicity. We assume $\lambda_{\Phi\sigma_i} < 0$ ($i = 1, 2$) and $\lambda_{\Phi, \sigma_1, \sigma_2} > 0$.

Around the vacuum, the scalar fields are decomposed as

$$\Phi = \begin{pmatrix} H^+ \\ v_{\text{EW}} + \frac{1}{\sqrt{2}}(\hat{H} + ia) \end{pmatrix} , \quad \sigma_i = v_i + \frac{1}{\sqrt{2}}(\hat{S}_i + i\hat{A}_i) , \quad (i = 1, 2) . \tag{A20}$$

In this case, H^+ , a , and a linear combination of $\hat{A}_{1,2}$ are would-be Goldstone modes, which are set to zero in the unitary gauge.

From $\partial V / \partial \hat{H} = \partial V / \partial \hat{S}_i = 0$, we find

$$\mu_\Phi^2 = 2\lambda_H v_{\text{EW}}^2 + \lambda_{\Phi\sigma_1} v_1^2 + \lambda_{\Phi\sigma_2} v_2^2 , \tag{A21}$$

$$\mu_{\sigma_1}^2 = 2\lambda_{\sigma_1} v_1^2 + \lambda_{\Phi\sigma_1} v_{\text{EW}}^2 - 2c v_2 , \tag{A22}$$

$$\mu_{\sigma_2}^2 = 2\lambda_{\sigma_2} v_2^2 + \lambda_{\Phi\sigma_2} v_{\text{EW}}^2 - c \frac{v_1^2}{v_2} . \tag{A23}$$

The squared mass matrix of the CP-even scalars are given by,

$$M^2 = \begin{pmatrix} 4\lambda_\Phi v_{\text{EW}}^2 & 2\lambda_{\Phi\sigma_1} v_1 v_{\text{EW}} & 2\lambda_{\Phi\sigma_2} v_2 v_{\text{EW}} \\ 2\lambda_{\Phi\sigma_1} v_1 v_{\text{EW}} & 4\lambda_{\sigma_1} v_1^2 & -2cv_1 \\ 2\lambda_{\Phi\sigma_2} v_2 v_{\text{EW}} & -2cv_1 & \frac{cv_1^2}{v_2} + 4\lambda_{\sigma_2} v_2^2 \end{pmatrix}, \quad (\text{A24})$$

in the $(\hat{H}, \hat{S}_1, \hat{S}_2)$ basis. As we are interested in the case where $\lambda_\Phi \gg |\lambda_{\Phi\sigma_i}|, \lambda_{\sigma_i}$ ($i = 1, 2$), we can approximately diagonalize the matrix by,

$$\hat{H} = H - \theta_1 \tilde{S}_1 - \theta_2 \tilde{S}_2, \quad (\text{A25})$$

$$\hat{S}_1 = \tilde{S}_1 + \theta_1 H, \quad (\text{A26})$$

$$\hat{S}_2 = \tilde{S}_2 + \theta_2 H, \quad (\text{A27})$$

where the small mixing angles are given by,

$$\theta_i \simeq \frac{1}{2} \frac{\lambda_{\Phi\sigma_i} v_i v_{\text{EW}}}{\lambda_H v_{\text{EW}}^2 - \lambda_{\sigma_i} v_i^2} \simeq \frac{2\lambda_{\Phi\sigma_i} v_i v_{\text{EW}}}{m_H^2}, \quad (\text{A28})$$

for $i = 1, 2$ with small multiplicative correction factors of $\mathcal{O}(\lambda_{\Phi\sigma_i}, cv_i/m_H, \lambda_{\sigma_i})$. To the leading order of $\lambda_{\Phi\sigma_i}, cv_i/m_H, \lambda_{\sigma_i}$, the squared mass matrix of $(\tilde{S}_1, \tilde{S}_2)$ is given by,

$$M_S^2 \simeq \begin{pmatrix} 4\lambda_{\sigma_1} v_1^2 & -2cv_1 \\ -2cv_1 & \frac{cv_1^2}{v_2} + 4\lambda_{\sigma_2} v_2^2 \end{pmatrix}. \quad (\text{A29})$$

We define the mass eigenstates of M_S^2 as (S_1, S_2) whose masses are denoted by m_{S_1} and m_{S_2} .

The squared mass matrix of the CP-odd scalars is given by,

$$M_A^2 = \begin{pmatrix} 4cv_2 & -2cv_1 \\ -2cv_1 & c \frac{v_1^2}{v_2} \end{pmatrix}, \quad (\text{A30})$$

in the (\hat{A}_1, \hat{A}_2) basis. The matrix can be diagonalized by

$$\begin{pmatrix} A \\ P \end{pmatrix} = \begin{pmatrix} \cos \alpha & \sin \alpha \\ -\sin \alpha & \cos \alpha \end{pmatrix} \begin{pmatrix} \hat{A}_1 \\ \hat{A}_2 \end{pmatrix}, \quad (\text{A31})$$

where

$$\sin \alpha = \frac{2v_2}{\sqrt{v_1^2 + 4v_2^2}}, \quad \cos \alpha = \frac{v_1}{\sqrt{v_1^2 + 4v_2^2}}. \quad (\text{A32})$$

Here, A corresponds to the massless would-be Goldstone mode, while the mass of P is given by,

$$m_P^2 = \frac{c(v_1^2 + 4v_2^2)}{v_2}. \quad (\text{A33})$$

After eliminating the mixings to \hat{S}_i 's, the Higgs couplings to the scalar sector are given by,

$$\mathcal{L} = \sum_{i=1,2} \left(-\frac{1}{2} g_{H\tilde{S}_i\tilde{S}_i} H \tilde{S}_i^2 - \frac{1}{2} g_{H\hat{A}_i\hat{A}_i} H \hat{A}_i^2 \right), \quad (\text{A34})$$

where

$$g_{H\tilde{S}_i\tilde{S}_i} = g_{H\hat{A}_i\hat{A}_i} = \frac{1}{\sqrt{2}} \frac{m_H^2}{v_i} \times \theta_i. \quad (\text{A35})$$

The absence of $H\tilde{S}_1\tilde{S}_2$ and $H\hat{A}_1\hat{A}_2$ is due to our simplification that we have omitted the

$|\sigma_1|^2|\sigma_2|^2$ term. The Higgs couplings to Z' 's and P are, on the other hand, given by

$$\begin{aligned} \mathcal{L} = & -\sqrt{2}g_{Z'}^2(v_1\theta_1 + 4v_2\theta_2)HZ'_\mu Z'^\mu - \frac{m_H^2}{2\sqrt{2}}\left(s_\alpha^2\frac{\theta_1}{v_1} + c_\alpha^2\frac{\theta_2}{v_2}\right)HP^2 \\ & - g_{Z'}(s_\alpha\theta_1 - 2c_\alpha\theta_2)(P\partial_\mu HZ'^\mu - H\partial_\mu PZ'^\mu) , \end{aligned} \quad (\text{A36})$$

$$\begin{aligned} = & -\frac{1}{2}\frac{\sqrt{2}m_{Z'}^2}{v_1^2 + 4v_2^2}(v_1\theta_1 + 4v_2\theta_2)HZ'_\mu Z'^\mu - \frac{1}{2\sqrt{2}}\frac{m_H^2}{v_1 + 4v_2^2}\left(4v_2^2\frac{\theta_1}{v_1} + v_1^2\frac{\theta_2}{v_2}\right)HP^2 \\ & - \frac{\sqrt{2}m_{Z'}v_1v_2}{v_1^2 + 4v_2^2}\left(\frac{\theta_1}{v_1} - \frac{\theta_2}{v_2}\right)(P\partial_\mu HZ'^\mu - H\partial_\mu PZ'^\mu) , \end{aligned} \quad (\text{A37})$$

where $s_\alpha \equiv \sin \alpha$ and $c_\alpha \equiv \cos \alpha$.

As in the case of the single scalar model, $S_{1,2}$ dominantly decay into a pair of Z' 's. As we will see below, P can decay into a CP-even scalar and Z' . Thus, the branching ratio of the invisible Higgs decay is given by,

$$\text{Br}(H \rightarrow \text{invisible}) = \frac{\Gamma_{H \rightarrow Z'Z'} + \Gamma_{H \rightarrow SS} + \Gamma_{H \rightarrow PP} + \Gamma_{H \rightarrow Z'P}}{\Gamma_{\text{SM}} + \Gamma_{H \rightarrow Z'Z'} + \Gamma_{H \rightarrow SS} + \Gamma_{H \rightarrow PP} + \Gamma_{H \rightarrow Z'P}} , \quad (\text{A38})$$

where $\Gamma_{H \rightarrow SS}$ denotes the sum of the decay rates into the CP-even scalars (S_1, S_2). For $m_H \gg m_{Z'}, m_{S_1}, m_{S_2}, m_P$, we find¹⁶

$$\Gamma_{H \rightarrow Z'Z'} + \Gamma_{H \rightarrow SS} + \Gamma_{H \rightarrow PP} + \Gamma_{H \rightarrow Z'P} \simeq \frac{(|\lambda_{\Phi\sigma_1}|^2 + |\lambda_{\Phi\sigma_2}|^2)v_{\text{EW}}^2}{8\pi m_H} . \quad (\text{A40})$$

As a result, the upper limit on the branching fraction of Higgs invisible decay mode, $\text{Br}(H \rightarrow \text{invisible}) < 0.11$ [64], results in a constraint,

$$(|\lambda_{\Phi\sigma_1}|^2 + |\lambda_{\Phi\sigma_2}|^2)^{1/2} < 7 \times 10^{-3} , \quad (\text{A41})$$

for the two scalar models (see Eq. (A18)).

¹⁶ Note that

$$\Gamma_{H \rightarrow Z'Z'} + \Gamma_{H \rightarrow PP} + \Gamma_{H \rightarrow Z'P} = \Gamma_{H \rightarrow \hat{A}_1 + \hat{A}_1} + \Gamma_{H \rightarrow \hat{A}_2 + \hat{A}_2} , \quad (\text{A39})$$

in the limit of $m_H \gg m_P$, which is in agreement with the Goldstone equivalence theorem.

Finally, let us comment on the fate of the CP-odd scalar P . Through the interactions,

$$\mathcal{L} = g_{Z's_\alpha} P \partial_\mu \tilde{S}_1 Z'^\mu - g_{Z's_\alpha} \tilde{S}_1 \partial_\mu P Z'^\mu - 2g_{Z'c_\alpha} P \partial_\mu \tilde{S}_2 Z'^\mu + 2g_{Z'c_\alpha} \tilde{S}_2 \partial_\mu P Z'^\mu , \quad (\text{A42})$$

P decays into Z' and a CP-even scalar when kinematically allowed. In such a case, the decay rate of P is comparable to those of the CP-even scalars in Fig. 4 for $m_P = \mathcal{O}(m_{S_i})$. For example, for

$$v_1 = 80 \text{ GeV} , \quad v_2 = 50 \text{ GeV} , \quad c = 0.03 \text{ GeV} , \quad (\text{A43})$$

$$\lambda_{\sigma_1} = \lambda_{\sigma_2} = 3 \times 10^{-4} , \quad \lambda_{\Phi\sigma_1} = \lambda_{\Phi\sigma_2} = 3 \times 10^{-3} , \quad (\text{A44})$$

we obtain

$$m_{S_1} = 3.5 \text{ GeV} , \quad m_{S_2} = 1.4 \text{ GeV} , \quad m_P = 3.1 \text{ GeV} , \quad (\text{A45})$$

which allows $P \rightarrow Z' + S_2$. Hence, P does not cause any cosmological problems for $m_P = \mathcal{O}(1) \text{ GeV}$.

When P is lighter than both the CP-even scalars, P decays into $Z'Z'Z'$ through a virtual CP-even scalar. In this case, the decay rate of P is expected to be roughly suppressed by $\lambda_{\sigma_i}^2 m_P^4 / (8\pi m_{S_i}^4)$ compared to the two-body decay rate in Fig. 4. Even in such a case, P does not cause cosmological problems as long as its decay temperature, $T_D \simeq \sqrt{\Gamma_P M_P}$, is much higher than $\mathcal{O}(10) \text{ MeV}$.

Appendix B: Finite density effect

In this appendix, we derive an effective mass of a scalar field that couples to the particles with finite densities. For simplicity, let us consider a model where a complex scalar field σ couples to a real scalar field χ that has finite density. The Lagrangian density of them is

assumed to be

$$\mathcal{L} = |\partial_\mu \sigma|^2 + \frac{1}{2}(\partial_\mu \chi)^2 - V , \quad (\text{B1})$$

$$V = \lambda_\sigma(|\sigma|^2 - v^2)^2 + \frac{1}{2}m_\chi^2\chi^2 + \frac{\kappa}{2}\chi^2|\sigma|^2 , \quad (\text{B2})$$

where λ_σ and κ are dimensionless coupling constants, and v and m_χ are the parameters with mass dimension one. We assume $\lambda_\sigma > 0$ so that the scalar potential of σ is bounded from below. In general, the sign of κ can be positive or negative. In this model, σ obtains a non-vanishing expectation value at the vacuum, which breaks the global U(1) symmetry of σ .

Let us consider a system with a finite volume $V_{3\text{D}} = L^3$, where L is a large length scale. The mode expansion of χ is then given by,

$$\hat{\chi}(x) = \frac{1}{L^{3/2}} \sum_{\mathbf{n}} \frac{1}{\sqrt{2p^0}} (\hat{a}_{\mathbf{n}} e^{-ipx} + \hat{a}_{\mathbf{n}}^\dagger e^{ipx}) , \quad (\text{B3})$$

where $\mathbf{n} = (n_1, n_2, n_3)$ is a set of three integers, with which the 3D momentum of χ is given by,

$$\mathbf{p} = \frac{2\pi}{L} \mathbf{n} . \quad (\text{B4})$$

The creation and annihilation operators satisfy

$$[\hat{a}_{\mathbf{n}}, \hat{a}_{\mathbf{n}'}^\dagger] = \delta_{\mathbf{n}\mathbf{n}'} . \quad (\text{B5})$$

Let us assume that the number density of χ is $n_\chi \neq 0$, which is given by

$$n_\chi = \frac{1}{V_{3\text{D}}} \sum_{\mathbf{n}} N_{\mathbf{n}} , \quad (\text{B6})$$

where $N_{\mathbf{n}}$ is the particle number for each mode in the 3D volume $V_{3\text{D}}$. The corresponding

particle state of $\hat{\chi}$ is given by,

$$|n_\chi\rangle = \prod_{\mathbf{n}} \left[\frac{1}{\sqrt{N_{\mathbf{n}}!}} (\hat{a}_{\mathbf{n}}^\dagger)^{N_{\mathbf{n}}} \right] |0\rangle , \quad (\text{B7})$$

where

$$\langle 0|0\rangle = 1 , \quad (\text{B8})$$

$$\langle n_\chi|n_\chi\rangle = 1 . \quad (\text{B9})$$

In this state, the expectation value of $\chi^2(x)$ is given by

$$\langle n_\chi | [\hat{\chi}^2(x)]_{\text{R}} | n_\chi \rangle = \sum_{\mathbf{n}, \mathbf{n}'} \frac{2}{L^3 (2p_0 2p'_0)^{1/2}} \langle n_\chi | a_{\mathbf{n}}^\dagger a_{\mathbf{n}'} e^{-i(p-p')x} | n_\chi \rangle , \quad (\text{B10})$$

$$= \sum_{\mathbf{n}} \frac{N_{\mathbf{n}}}{L^3 p_0} , \quad (\text{B11})$$

$$= n_\chi \langle p_0^{-1} \rangle . \quad (\text{B12})$$

Note that we define the renormalized operator $[\hat{\chi}^2(x)]_{\text{R}}$ by

$$[\hat{\chi}^2(x)]_{\text{R}} \equiv \hat{\chi}^2(x) - \langle 0 | \chi^2(x) | 0 \rangle . \quad (\text{B13})$$

Now consider the effective mass of σ around its origin,

$$m_{\text{eff}}^2 = \left. \frac{\partial^2 V}{\partial \sigma^* \partial \sigma} \right|_{\sigma=0} = -2\lambda_\sigma v^2 + \frac{1}{2} \kappa \langle [\chi^2]_{\text{R}} \rangle \quad (\text{B14})$$

$$= -2\lambda_\sigma v^2 + \frac{1}{2} \kappa n_\chi \langle p_0^{-1} \rangle . \quad (\text{B15})$$

Thus, for $\kappa > 0$, the effective mass of σ becomes positive for

$$n_\chi > \frac{4\lambda_\sigma}{\kappa} \frac{v^2}{\langle p_0^{-1} \rangle} , \quad (\text{B16})$$

and hence, the $U(1)$ symmetry of σ is restored due to the finite density effect. When χ is thermalized, for example, the above mass term reproduces the thermal mass

$$m_{\text{th}}^2|_{\chi} = \frac{\kappa}{24} T^2 . \quad (\text{B17})$$

Now, let us apply this result to the $U(1)_{L_{\mu}-L_{\tau}}$ model. In this case, σ couples to the $U(1)_{L_{\mu}-L_{\tau}}$ gauge boson, which is expected to have a finite density in the early universe. The relevant coupling is

$$\mathcal{L} = |D_{\mu}\sigma|^2 \supset g^2 A_{\mu} A^{\mu} |\sigma|^2 \rightarrow -g^2 A_i A_i |\sigma|^2 , \quad (\text{B18})$$

where we take the unitary gauge. Thus, σ couples to the finite density particle with $\kappa = 2g^2 > 0$, and hence, we find that the $U(1)$ symmetry of σ can be restored by the finite density of the gauge boson.

Let us also comment that the finite density of σ itself can also contribute to the effective mass of σ . Since the quartic coupling constant λ_{σ} is required to be positive to avoid the potential unbounded from below. Thus, the finite density of σ also can restore the symmetry. In the case of the thermalized σ , the finite density effects on the mass reduce to the thermal mass,

$$m_{\text{th}}^2|_{\sigma} = \frac{\lambda_{\sigma}}{3} T^2 . \quad (\text{B19})$$

Appendix C: Mass basis of right-handed neutrinos

Here, we introduce the mass basis of the right-handed neutrinos in the $U(1)_{L_{\mu}-L_{\tau}}$ broken phase and summarize the Lagrangian for four-component fermions in the mass basis. This Lagrangian will be used to evaluate the asymmetry parameters in the Appendix D. On the notations of fermions, we follow Ref. [35].

First, we consider the mass basis in the $U(1)_{L_{\mu}-L_{\tau}}$ broken phase. In terms of two-

component fermions, the Lagrangian related to right-handed neutrinos is given by

$$\begin{aligned} \mathcal{L} = & i\bar{N}_\alpha^\dagger \bar{\sigma}^\mu D_\mu \bar{N}_\alpha + \left(-\frac{M_{R\alpha\beta}}{2} \bar{N}_\alpha \bar{N}_\beta - \lambda_{\nu\alpha\beta} L_\alpha \tilde{\Phi} \bar{N}_\beta - h_{e\mu} \sigma_1 \bar{N}_e \bar{N}_\mu - h_{e\tau} \sigma_1^* \bar{N}_e \bar{N}_\tau \right. \\ & \left. - \frac{1}{2} h_{\mu\mu} \sigma_2 \bar{N}_\mu \bar{N}_\mu - \frac{1}{2} h_{\tau\tau} \sigma_2^* \bar{N}_\tau \bar{N}_\tau + \text{h.c.} \right) . \end{aligned} \quad (\text{C1})$$

When the $U(1)_{L_\mu-L_\tau}$ symmetry is spontaneously broken due to nonzero $\langle \sigma_{1,2} \rangle$, the Majorana mass term receives additional contributions from the Majorana Yukawa terms as

$$M_{R,\text{eff}} = \begin{pmatrix} M_{ee} & h_{e\mu} \langle \sigma_1 \rangle & h_{e\tau} \langle \sigma_1 \rangle \\ h_{e\mu} \langle \sigma_1 \rangle & h_{\mu\mu} \langle \sigma_2 \rangle & M_{\mu\tau} \\ h_{e\tau} \langle \sigma_1 \rangle & M_{\mu\tau} & h_{\tau\tau} \langle \sigma_2 \rangle \end{pmatrix} . \quad (\text{C2})$$

Thus, either of \bar{N}_α is not the mass eigenstates in general. Since $M_{R,\text{eff}}$ is a complex symmetric matrix, it is diagonalized by a unitary matrix Ω using the Autonne-Takagi factorization as

$$M'_{R,\text{eff}} \equiv \begin{pmatrix} M_1 & 0 & 0 \\ 0 & M_2 & 0 \\ 0 & 0 & M_3 \end{pmatrix} = \Omega^T M_{R,\text{eff}} \Omega . \quad (\text{C3})$$

Here, M_I is the mass eigenvalue with $I = 1, 2, 3$ and we choose Ω so that M_I is real and $M_1 \leq M_2 \leq M_3$ without loss of generality. Thus, the Majorana mass term is diagonalized as

$$\bar{N}^T \frac{M_{R,\text{eff}}}{2} \bar{N} = \bar{N}'^T \frac{M'_{R,\text{eff}}}{2} \bar{N}' , \quad (\text{C4})$$

where $\bar{N}'_I \equiv \Omega_{I\alpha}^\dagger \bar{N}_\alpha$ represents the mass eigenstates.

Using this mass basis, we rewrite the Lagrangian in Eq. (C1) as

$$\begin{aligned} \mathcal{L}' = i\bar{N}_I^{\dagger}\bar{\sigma}^{\mu}D'_{\mu IJ}\bar{N}'_J - \left(\frac{M'_{R,\text{eff}IJ}}{2}\bar{N}'_I\bar{N}'_J + \lambda'_{\nu\alpha I}L_{\alpha}\tilde{\Phi}\bar{N}'_I + \frac{1}{2}H_{IJ}^{e\mu\nu}\delta\sigma_1\bar{N}'_I\bar{N}'_J + \frac{1}{2}H_{IJ}^{e\tau\nu}\delta\sigma_1^*\bar{N}'_I\bar{N}'_J \right. \\ \left. + \frac{1}{2}H_{IJ}^{\mu\mu\nu}\delta\sigma_2\bar{N}'_I\bar{N}'_J + \frac{1}{2}H_{IJ}^{\tau\tau\nu}\delta\sigma_2^*\bar{N}'_I\bar{N}'_J + \text{h.c.} \right) . \end{aligned} \quad (\text{C5})$$

Here,

$$\delta\sigma_i \equiv \sigma_i - \langle\sigma_i\rangle = \frac{1}{\sqrt{2}}\left(\hat{S}_i + i\hat{A}_i\right) , \quad (\text{C6})$$

and the covariant derivative is given by,

$$\begin{aligned} D'_{\mu IJ} &\equiv \partial_{\mu}\delta_{IJ} - ig_{Z'}Z'_{\mu}\Omega_{I\alpha}^{\dagger}Q_{\alpha\beta}^{\text{f}}\Omega_{\beta J} \\ &\equiv \partial_{\mu}\delta_{IJ} - ig_{Z'}Z'_{\mu}Q'_{IJ} , \end{aligned} \quad (\text{C7})$$

with

$$Q^{\text{f}} \equiv \begin{pmatrix} 0 & 0 & 0 \\ 0 & 1 & 0 \\ 0 & 0 & -1 \end{pmatrix} . \quad (\text{C8})$$

The Dirac Yukawa couplings are given by

$$\lambda'_{\nu\alpha I} = \lambda_{\nu\alpha\beta}\Omega_{\beta I} , \quad (\text{C9})$$

and the Majorana Yukawa couplings are represented by the matrices:

$$H^{\alpha\beta I} = \Omega^{\text{T}}H^{\alpha\beta}\Omega , \quad (\text{C10})$$

with

$$H^{e\mu} \equiv \begin{pmatrix} 0 & h_{e\mu} & 0 \\ h_{e\mu} & 0 & 0 \\ 0 & 0 & 0 \end{pmatrix}, \quad H^{e\tau} \equiv \begin{pmatrix} 0 & 0 & h_{e\tau} \\ 0 & 0 & 0 \\ h_{e\tau} & 0 & 0 \end{pmatrix}, \quad (\text{C11})$$

$$H^{\mu\mu} \equiv \begin{pmatrix} 0 & 0 & 0 \\ 0 & h_{\mu\mu} & 0 \\ 0 & 0 & 0 \end{pmatrix}, \quad H^{\tau\tau} \equiv \begin{pmatrix} 0 & 0 & 0 \\ 0 & 0 & 0 \\ 0 & 0 & h_{\tau\tau} \end{pmatrix}. \quad (\text{C12})$$

Next, we rewrite the Lagrangian in terms of four-component fermions:

$$\Psi_\alpha \equiv \begin{pmatrix} \bar{N}_\alpha \\ \bar{N}_\alpha^\dagger \end{pmatrix}, \quad \Psi_{L_\alpha} \equiv \begin{pmatrix} L_\alpha \\ 0 \end{pmatrix}. \quad (\text{C13})$$

The mass eigenstates of right-handed neutrinos as four-component fermions are given by

$$\Psi'_I \equiv \Omega_{I\alpha}^\dagger \Psi_\alpha. \quad (\text{C14})$$

Then, the Lagrangian becomes

$$\mathcal{L}' = \mathcal{L}'_{\text{kin}} + \mathcal{L}'_{\text{mass}} + \mathcal{L}'_{\text{DY}} + \mathcal{L}'_{\text{MY}}, \quad (\text{C15})$$

with

$$\begin{aligned}\mathcal{L}'_{\text{kin}} &= \frac{i}{2} \bar{\Psi}'_I \not{D}_{IJ} \Psi'_J \\ &= \frac{i}{2} \bar{\Psi}'_I \gamma^\mu (\partial_\mu \delta_{IJ} - i g_{Z'} \gamma^5 Z'_\mu Q'_{IJ}) \Psi'_J ,\end{aligned}\tag{C16}$$

$$\mathcal{L}'_{\text{mass}} = -\frac{1}{2} \bar{\Psi}'_I (\text{Re}[M'_{R,\text{eff}}] - i \gamma^5 \text{Im}[M'_{R,\text{eff}}])_{IJ} \Psi'_J ,\tag{C17}$$

$$\mathcal{L}'_{\text{DY}} = -\lambda'_{\nu\alpha I} \bar{\Psi}'_I \tilde{\Phi} P_L \Psi_{L_\alpha} - \lambda'^*_{\nu\alpha I} \bar{\Psi}_{L_\alpha} P_R \tilde{\Phi}^\dagger \Psi'_I ,\tag{C18}$$

$$\mathcal{L}'_{\text{MY}} = - \sum_{X=\hat{S}_1, \hat{A}_1, \hat{S}_2, \hat{A}_2} \bar{\Psi}'_I F_{IJ}^X X \Psi'_J .\tag{C19}$$

Here,

$$F_{IJ}^{\hat{S}_1} \equiv \frac{(\text{Re}[H^{e\mu\prime} + H^{e\tau\prime}] - i \gamma^5 \text{Im}[H^{e\mu\prime} + H^{e\tau\prime}])_{IJ}}{2\sqrt{2}} ,\tag{C20}$$

$$F_{IJ}^{\hat{A}_1} \equiv \frac{(\text{Re}[i(H^{e\mu\prime} - H^{e\tau\prime})] - i \gamma^5 \text{Im}[i(H^{e\mu\prime} - H^{e\tau\prime})])_{IJ}}{2\sqrt{2}} ,\tag{C21}$$

$$F_{IJ}^{\hat{S}_2} \equiv \frac{(\text{Re}[H^{\mu\mu\prime} + H^{\tau\tau\prime}] - i \gamma^5 \text{Im}[H^{\mu\mu\prime} + H^{\tau\tau\prime}])_{IJ}}{2\sqrt{2}} ,\tag{C22}$$

$$F_{IJ}^{\hat{A}_2} \equiv \frac{(\text{Re}[i(H^{\mu\mu\prime} - H^{\tau\tau\prime})] - i \gamma^5 \text{Im}[i(H^{\mu\mu\prime} - H^{\tau\tau\prime})])_{IJ}}{2\sqrt{2}} .\tag{C23}$$

For later convenience, we also define

$$F_{IJ}^X \equiv \frac{1}{2\sqrt{2}} (f_{IJ}^X - i \gamma^5 g_{IJ}^X) .\tag{C24}$$

Appendix D: Asymmetry parameters

Using the Lagrangian in the Appendix C, we evaluate the asymmetry parameters in the decays of the right-handed neutrinos. In particular, we consider the decays of

$$\Psi'_I \rightarrow \Psi_{L_\alpha} \tilde{\Phi} ,\tag{D1}$$

$$\Psi'_I \rightarrow \Psi_{L_\alpha}^c \tilde{\Phi}^\dagger .\tag{D2}$$

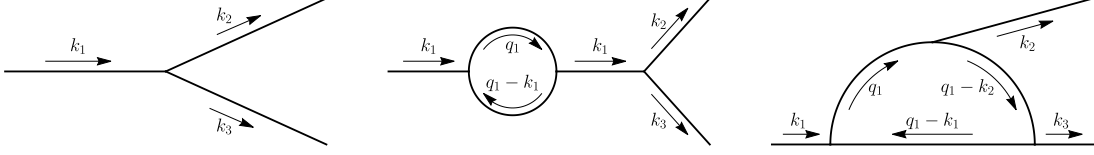


Figure 5. *Momentum assignment in tree, wave-function, and vertex diagrams.*

To evaluate the asymmetry parameters, we consider tree (Fig. 6) and one-loop (Figs. 7–11) diagrams. The one-loop diagrams are classified into wave-function and vertex diagrams. The assignment of the momenta in the following calculations is shown in Fig. 5. Hereafter, we approximate that the particles other than the right-handed neutrinos are massless. We also take the leading order of $\lambda_{\Phi\sigma_i}$ and cv_i/m_H . In other words, we ignore the mixings among the Higgs and $\hat{S}_{1,2}$ and identify $\hat{S}_{1,2}$ with the mass eigenstates $S_{1,2}$. The CP-odd scalars \hat{A}_1 and \hat{A}_2 are related to the physical degree of freedom P by

$$\hat{A}_1 = -P \sin \alpha, \quad \hat{A}_2 = P \cos \alpha, \quad (\text{D3})$$

where we neglect the would-be Goldstone mode, A (see also the Appendix A).

First, we consider the tree diagrams in Fig. 6. The amplitudes of these processes are given by

$$i\mathcal{M}_{\text{tree}} = \bar{u}(-i\lambda'_{\nu\alpha I} P_R)u, \quad (\text{D4})$$

$$i\overline{\mathcal{M}}_{\text{tree}} = \bar{u}(-i\lambda'_{\nu\alpha I} P_L)u. \quad (\text{D5})$$

The decay rate of right-handed neutrinos through these processes is proportional to

$$|\mathcal{M}_{\text{tree}}|^2 + |\overline{\mathcal{M}}_{\text{tree}}|^2 = 2[\lambda_\nu'^\dagger \lambda_\nu']_{II} \bar{u} P_L u \bar{u} P_R u \quad (\text{D6})$$

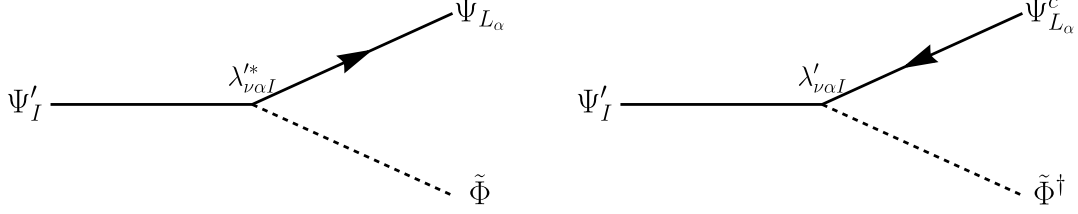


Figure 6. Tree diagrams for decays of right-handed neutrinos. Plain solid lines, solid lines with arrows, and dashed lines correspond to right-handed neutrinos, left-handed leptons, and scalar bosons, respectively.

1. Wave-function diagram with $\Psi_L\Phi$ loop

The diagrams with $\Psi_{L\beta}$ loop in the upper side of Fig. 7 give

$$i\mathcal{M}_a^L = \bar{u}(-i\lambda_{\nu\alpha J}^* P_R) \frac{i(k_1 + M_J)}{k_1^2 - M_J^2} (-i\lambda'_{\nu\beta J} P_L) n_w \int \frac{d^4 q_1}{(2\pi)^4} \frac{i\not{q}_1}{q_1^2} \frac{i}{(q_1 - k_1)^2} (-i\lambda_{\nu\beta I}^* P_R) u, \quad (\text{D7})$$

$$i\overline{\mathcal{M}}_a^L = \bar{u}(-i\lambda'_{\nu\alpha J} P_L) \frac{i(k_1 + M_J)}{k_1^2 - M_J^2} (-i\lambda_{\nu\beta J}^* P_L) n_w \int \frac{d^4 q_1}{(2\pi)^4} \frac{i\not{q}_1}{q_1^2} \frac{i}{(q_1 - k_1)^2} (-i\lambda_{\nu\beta I}^* P_R) u, \quad (\text{D8})$$

where $n_w = 2$ represents the degree of freedom of the $SU(2)$ doublet in the loop.

The diagrams with $\Psi_{L\beta}^c$ loop in the lower side of Fig. 7 give

$$i\mathcal{M}_a^{L^c} = \bar{u}(-i\lambda_{\nu\alpha J}^* P_R) \frac{i(k_1 + M_J)}{k_1^2 - M_J^2} (-i\lambda_{\nu\beta J}^* P_R) n_w \int \frac{d^4 q_1}{(2\pi)^4} \frac{i\not{q}_1}{q_1^2} \frac{i}{(q_1 - k_1)^2} (-i\lambda'_{\nu\beta I} P_L) u, \quad (\text{D9})$$

$$i\overline{\mathcal{M}}_a^{L^c} = \bar{u}(-i\lambda'_{\nu\alpha J} P_L) \frac{i(k_1 + M_J)}{k_1^2 - M_J^2} (-i\lambda_{\nu\beta J}^* P_R) n_w \int \frac{d^4 q_1}{(2\pi)^4} \frac{i\not{q}_1}{q_1^2} \frac{i}{(q_1 - k_1)^2} (-i\lambda'_{\nu\beta I} P_L) u. \quad (\text{D10})$$

As discussed in Sec. V A, the asymmetry parameters are proportional to the imaginary part coming from loop integrals. Thus, we pick up the imaginary part in the loop integrals

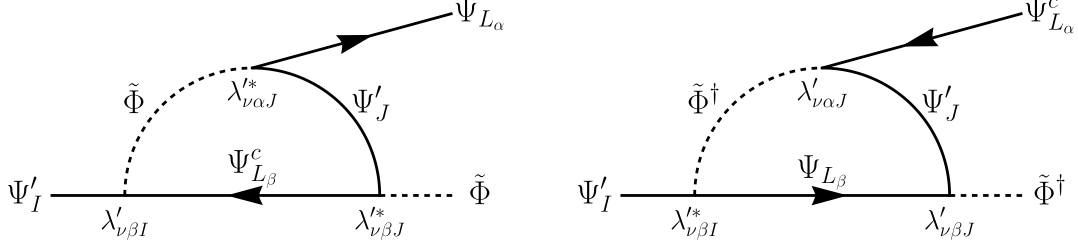


Figure 8. Vertex diagrams with $\Psi_L \Phi \Psi'$ loop for decays of right-handed neutrinos.

where we introduce the regulator with $\Gamma_{\text{tree},J}^2$ reflecting the finite width of the right-handed neutrinos [69].

2. Vertex diagram with $\Psi_L \Phi \Psi'$ loop

The vertex diagrams with $\Psi_L \Phi \Psi'$ loop in Fig. 8 give

$$i\mathcal{M}_b = \bar{u}(-i\lambda'_{\nu\alpha J}P_R) \int \frac{d^4q_1}{(2\pi)^4} \frac{i(\not{k}_2 - \not{q}_1 + M_J)}{(q_1 - k_2)^2 - M_J^2} (-i\lambda'_{\nu\beta J}P_R) \frac{i(\not{k}_1 - \not{q}_1)}{(q_1 - k_1)^2} (-i\lambda'_{\nu\beta I}P_L) \frac{i}{q_1^2} u, \quad (\text{D17})$$

$$i\overline{\mathcal{M}}_b = \bar{u}(-i\lambda'_{\nu\alpha J}P_L) \int \frac{d^4q_1}{(2\pi)^4} \frac{i(\not{k}_2 - \not{q}_1 + M_J)}{(q_1 - k_2)^2 - M_J^2} (-i\lambda'_{\nu\beta J}P_L) \frac{i(\not{k}_1 - \not{q}_1)}{(q_1 - k_1)^2} (-i\lambda'_{\nu\beta I}P_R) \frac{i}{q_1^2} u. \quad (\text{D18})$$

Note that \mathcal{M}_b does not include n_w .

As in the case of diagram (a), we pick the imaginary part in the loop integrals and obtain

$$\mathcal{M}_b \supset \frac{ir_J}{16\pi} \lambda'_{\nu\alpha J} [\lambda_\nu^\dagger \lambda'_\nu]_{JI} (1 + (1 + r_J^2) \log r_J^2 - (1 + r_J^2) \log(1 + r_J^2)) \bar{u} P_R u, \quad (\text{D19})$$

$$\overline{\mathcal{M}}_b \supset \frac{ir_J}{16\pi} \lambda'_{\nu\alpha J} [\lambda_\nu'^T \lambda_\nu^*]_{JI} (1 + (1 + r_J^2) \log r_J^2 - (1 + r_J^2) \log(1 + r_J^2)) \bar{u} P_R u. \quad (\text{D20})$$

As a result, the asymmetry parameter from diagram (b) is given by

$$\epsilon_I^{(b)} = -\frac{1}{8\pi} \sum_J \frac{\text{Im}[[\lambda_\nu^\dagger \lambda'_\nu]_{IJ}^2]}{[\lambda_\nu^\dagger \lambda'_\nu]_{II}} r_J \left[1 - (1 + r_J^2) \log \left(\frac{1 + r_J^2}{r_J^2} \right) \right], \quad (\text{D21})$$

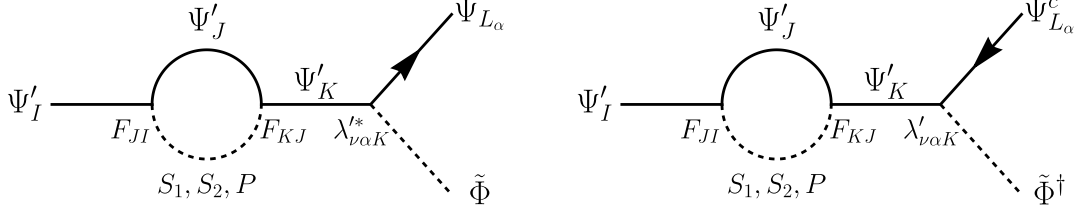


Figure 9. Wave-function diagrams with $\Psi'X$ loop for decays of right-handed neutrinos.

where $r_J \equiv M_J/M_I$.

3. Wave-function diagram with $\Psi'X$ loop

The wave-function diagrams with $\Psi'X$ loop in Fig. 9 give

$$i\mathcal{M}_c^X = \bar{u}(-i\lambda'_{\nu\alpha K}P_R)\frac{i(\not{k}_1 + M_K)}{k_1^2 - M_K^2}(-iF_{KJ}^X) \int \frac{d^4q_1}{(2\pi)^4} \frac{i(\not{q}_1 + M_J)}{q_1^2 - M_J^2} \frac{i}{(q_1 - k_1)^2 - M_X^2}(-iF_{JI}^X)u, \quad (\text{D22})$$

$$i\overline{\mathcal{M}}_c^X = \bar{u}(-i\lambda'_{\nu\alpha K}P_L)\frac{i(\not{k}_1 + M_K)}{k_1^2 - M_K^2}(-iF_{KJ}^X) \int \frac{d^4q_1}{(2\pi)^4} \frac{i(\not{q}_1 + M_J)}{q_1^2 - M_J^2} \frac{i}{(q_1 - k_1)^2 - M_X^2}(-iF_{JI}^X)u, \quad (\text{D23})$$

where $X = S_1, S_2, P$ is the scalar particle in the loop.

The loop integral in \mathcal{M}_c and $\overline{\mathcal{M}}_c$ has a nonzero imaginary part only when $M_I > M_J$ as expected from the optical theorem. For $M_I > M_J$, we pick the imaginary part in the loop

integrals and obtain

$$\begin{aligned} \mathcal{M}_c^X \supset \frac{i\lambda_{\nu\alpha K}^*(M_I^2 - M_J^2)}{256\pi M_I^3(M_I^2 - M_K^2)} & \left[(M_I - M_J)^2 g_{IJ}^X \{ (M_I + M_K) g_{JK}^X - i f_{JK}^X (M_I - M_K) \} \right. \\ & \left. + (M_I + M_J)^2 f_{IJ}^X \{ (M_I + M_K) f_{JK}^X + i g_{JK}^X (M_I - M_K) \} \right] \bar{u} P_R u , \end{aligned} \quad (\text{D24})$$

$$\begin{aligned} \overline{\mathcal{M}}_c^X \supset \frac{i\lambda'_{\nu\alpha K}(M_I^2 - M_J^2)}{256\pi M_I^3(M_I^2 - M_K^2)} & \left[(M_I - M_J)^2 g_{IJ}^X \{ (M_I + M_K) g_{JK}^X + i f_{JK}^X (M_I - M_K) \} \right. \\ & \left. + (M_I + M_J)^2 f_{IJ}^X \{ (M_I + M_K) f_{JK}^X - i g_{JK}^X (M_I - M_K) \} \right] \bar{u} P_L u . \end{aligned} \quad (\text{D25})$$

As a result, the difference between $|\mathcal{M}|^2$ and $|\overline{\mathcal{M}}|^2$ from diagram (c) is given by,

$$\begin{aligned} & (|\mathcal{M}|^2 - |\overline{\mathcal{M}}|^2)_c \\ &= \sum_{X=S_1, S_2, P} \frac{1 - r_J^2}{64\pi(1 - r_K^2)} \\ & \times \left[(1 + r_K) \{ \text{Im}\lambda'_{\nu\alpha I} \text{Re}\lambda'_{\nu\alpha K} - \text{Re}\lambda'_{\nu\alpha I} \text{Im}\lambda'_{\nu\alpha K} \} \{ (1 + r_J)^2 f_{IJ}^X f_{JK}^X + (1 - r_J)^2 g_{IJ}^X g_{JK}^X \} \right. \\ & \quad \left. + (1 - r_K) \{ \text{Re}\lambda'_{\nu\alpha I} \text{Re}\lambda'_{\nu\alpha K} + \text{Im}\lambda'_{\nu\alpha I} \text{Im}\lambda'_{\nu\alpha K} \} \{ (1 + r_J)^2 f_{IJ}^X g_{JK}^X - (1 - r_J)^2 g_{IJ}^X f_{JK}^X \} \right] \\ & \times \bar{u} P_L u \bar{u} P_R u . \end{aligned} \quad (\text{D26})$$

The corresponding asymmetry parameter is given by,

$$\begin{aligned} \epsilon_I^{(c)} &= \sum_{J, K} \frac{1 - r_J^2}{128\pi(1 - r_K^2)[\lambda_\nu^\dagger \lambda'_\nu]_{II}} \frac{(M_I^2 - M_K^2)^2}{(M_I^2 - M_K^2)^2 + M_I^2 \Gamma_{\text{tree}, K}^2} \Theta(M_I - M_J) \\ & \times \sum_{X=S_1, S_2, P} \left[-(1 + r_K) \text{Im}[\lambda_\nu^\dagger \lambda'_\nu]_{IJ} \{ (1 + r_J)^2 f_{IJ}^X f_{JK}^X + (1 - r_J)^2 g_{IJ}^X g_{JK}^X \} \right. \\ & \quad \left. + (1 - r_K) \text{Re}[\lambda_\nu^\dagger \lambda'_\nu]_{IJ} \{ (1 + r_J)^2 f_{IJ}^X g_{JK}^X - (1 - r_J)^2 g_{IJ}^X f_{JK}^X \} \right] , \end{aligned} \quad (\text{D27})$$

where we introduced the regulator again.

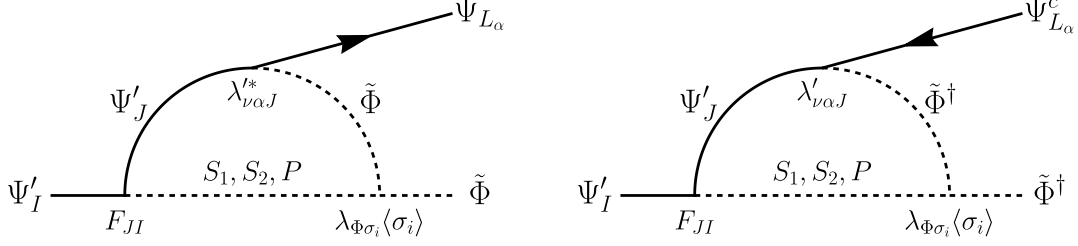


Figure 10. Vertex diagrams with $\Phi\Psi'X$ loop for decays of right-handed neutrinos.

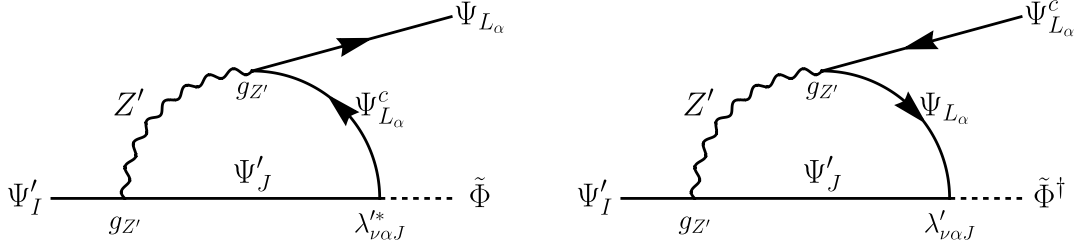


Figure 11. Vertex diagrams with $\Psi_L\Psi'Z'$ loop for decays of right-handed neutrinos. Wavy lines correspond to Z' .

4. Vertex diagram with $\Phi\Psi'X$ loop

The vertex diagrams with $\Phi\Psi'X$ loop in Fig. 10 include the scalar coupling proportional to $\lambda_{\Phi\sigma}\langle\sigma_i\rangle$. From the dimensional analysis, the contribution from this diagram is suppressed by $\langle\sigma_i\rangle/M_I$ compared with the contributions above. Moreover, $\lambda_{\Phi\sigma_i}$ is bounded from above as $\lambda_{\Phi\sigma_i} \lesssim 7 \times 10^{-3}$ as shown in the Appendix A while $\lambda'_{\nu\alpha I}$ and F_{IJ}^X are $\mathcal{O}(1)$ at most. Thus, the contribution of these diagrams to the total asymmetric parameter can be safely neglected.

5. Vertex diagram with $\Psi_L\Psi'Z'$ loop

The vertex diagrams with $\Psi_L\Psi'Z'$ loop in Fig. 11 include two of the gauge couplings $g_{Z'}$. Thus, the asymmetric parameter from these diagrams is suppressed by $g_{Z'}^2 \lesssim 10^{-6}$ and can be safely neglected.

-
- [1] G. W. Bennett *et al.* (Muon g-2), Phys. Rev. D **73**, 072003 (2006), arXiv:hep-ex/0602035.
 - [2] B. Abi *et al.* (Muon g-2), Phys. Rev. Lett. **126**, 141801 (2021), arXiv:2104.03281 [hep-ex].
 - [3] T. Albahri *et al.* (Muon g-2), Phys. Rev. D **103**, 072002 (2021), arXiv:2104.03247 [hep-ex].
 - [4] T. Aoyama *et al.*, Phys. Rept. **887**, 1 (2020), arXiv:2006.04822 [hep-ph].
 - [5] T. Aoyama, M. Hayakawa, T. Kinoshita, and M. Nio, Phys. Rev. Lett. **109**, 111808 (2012), arXiv:1205.5370 [hep-ph].
 - [6] T. Aoyama, T. Kinoshita, and M. Nio, Atoms **7**, 28 (2019).
 - [7] A. Czarnecki, W. J. Marciano, and A. Vainshtein, Phys. Rev. D **67**, 073006 (2003), [Erratum: Phys.Rev.D 73, 119901 (2006)], arXiv:hep-ph/0212229.
 - [8] C. Gnendiger, D. Stöckinger, and H. Stöckinger-Kim, Phys. Rev. D **88**, 053005 (2013), arXiv:1306.5546 [hep-ph].
 - [9] M. Davier, A. Hoecker, B. Malaescu, and Z. Zhang, Eur. Phys. J. C **77**, 827 (2017), arXiv:1706.09436 [hep-ph].
 - [10] A. Keshavarzi, D. Nomura, and T. Teubner, Phys. Rev. D **97**, 114025 (2018), arXiv:1802.02995 [hep-ph].
 - [11] G. Colangelo, M. Hoferichter, and P. Stoffer, JHEP **02**, 006 (2019), arXiv:1810.00007 [hep-ph].
 - [12] M. Hoferichter, B.-L. Hoid, and B. Kubis, JHEP **08**, 137 (2019), arXiv:1907.01556 [hep-ph].
 - [13] M. Davier, A. Hoecker, B. Malaescu, and Z. Zhang, Eur. Phys. J. C **80**, 241 (2020), [Erratum: Eur.Phys.J.C 80, 410 (2020)], arXiv:1908.00921 [hep-ph].
 - [14] A. Keshavarzi, D. Nomura, and T. Teubner, Phys. Rev. D **101**, 014029 (2020), arXiv:1911.00367 [hep-ph].
 - [15] A. Kurz, T. Liu, P. Marquard, and M. Steinhauser, Phys. Lett. B **734**, 144 (2014), arXiv:1403.6400 [hep-ph].
 - [16] K. Melnikov and A. Vainshtein, Phys. Rev. D **70**, 113006 (2004), arXiv:hep-ph/0312226.
 - [17] P. Masjuan and P. Sanchez-Puertas, Phys. Rev. D **95**, 054026 (2017), arXiv:1701.05829 [hep-ph].

- [18] G. Colangelo, M. Hoferichter, M. Procura, and P. Stoffer, JHEP **04**, 161 (2017), arXiv:1702.07347 [hep-ph].
- [19] M. Hoferichter, B.-L. Hoid, B. Kubis, S. Leupold, and S. P. Schneider, JHEP **10**, 141 (2018), arXiv:1808.04823 [hep-ph].
- [20] A. Gérardin, H. B. Meyer, and A. Nyffeler, Phys. Rev. D **100**, 034520 (2019), arXiv:1903.09471 [hep-lat].
- [21] J. Bijnens, N. Hermansson-Truedsson, and A. Rodríguez-Sánchez, Phys. Lett. B **798**, 134994 (2019), arXiv:1908.03331 [hep-ph].
- [22] G. Colangelo, F. Hagelstein, M. Hoferichter, L. Laub, and P. Stoffer, JHEP **03**, 101 (2020), arXiv:1910.13432 [hep-ph].
- [23] T. Blum, N. Christ, M. Hayakawa, T. Izubuchi, L. Jin, C. Jung, and C. Lehner, Phys. Rev. Lett. **124**, 132002 (2020), arXiv:1911.08123 [hep-lat].
- [24] G. Colangelo, M. Hoferichter, A. Nyffeler, M. Passera, and P. Stoffer, Phys. Lett. B **735**, 90 (2014), arXiv:1403.7512 [hep-ph].
- [25] R. L. Workman *et al.* (Particle Data Group), PTEP **2022**, 083C01 (2022).
- [26] F. V. Ignatov *et al.* (CMD-3), arXiv preprint (2023), arXiv:2302.08834 [hep-ex].
- [27] R. Foot, Mod. Phys. Lett. A **6**, 527 (1991).
- [28] X.-G. He, G. C. Joshi, H. Lew, and R. R. Volkas, Phys. Rev. D **44**, 2118 (1991).
- [29] R. Foot, X. G. He, H. Lew, and R. R. Volkas, Phys. Rev. D **50**, 4571 (1994), arXiv:hep-ph/9401250.
- [30] S. N. Gninenko and N. V. Krasnikov, Phys. Lett. B **513**, 119 (2001), arXiv:hep-ph/0102222.
- [31] S. Baek, N. G. Deshpande, X. G. He, and P. Ko, Phys. Rev. D **64**, 055006 (2001), arXiv:hep-ph/0104141.
- [32] B. Murakami, Phys. Rev. D **65**, 055003 (2002), arXiv:hep-ph/0110095.
- [33] E. Ma, D. P. Roy, and S. Roy, Phys. Lett. B **525**, 101 (2002), arXiv:hep-ph/0110146.
- [34] M. Bauer, P. Foldenauer, and J. Jaeckel, JHEP **07**, 094 (2018), arXiv:1803.05466 [hep-ph].
- [35] H. K. Dreiner, H. E. Haber, and S. P. Martin, Phys. Rept. **494**, 1 (2010), arXiv:0812.1594 [hep-ph].

- [36] K. Harigaya, T. Igari, M. M. Nojiri, M. Takeuchi, and K. Tobe, JHEP **03**, 105 (2014), arXiv:1311.0870 [hep-ph].
- [37] K. Asai, K. Hamaguchi, and N. Nagata, Eur. Phys. J. C **77**, 763 (2017), arXiv:1705.00419 [hep-ph].
- [38] K. Asai, K. Hamaguchi, N. Nagata, S.-Y. Tseng, and K. Tsumura, Phys. Rev. D **99**, 055029 (2019), arXiv:1811.07571 [hep-ph].
- [39] J. Heeck and W. Rodejohann, Phys. Rev. D **84**, 075007 (2011), arXiv:1107.5238 [hep-ph].
- [40] T. Araki, J. Heeck, and J. Kubo, JHEP **07**, 083 (2012), arXiv:1203.4951 [hep-ph].
- [41] P. Minkowski, Phys. Lett. **67B**, 421 (1977).
- [42] T. Yanagida, in *Horizontal gauge symmetry and masses of neutrinos*, Vol. 7902131 (1979) pp. 95–99.
- [43] S. L. Glashow, NATO Sci. Ser. B **61**, 687 (1980).
- [44] R. N. Mohapatra and G. Senjanovic, Phys. Rev. Lett. **44**, 912 (1980), [,231(1979)].
- [45] M. Gell-Mann, P. Ramond, and R. Slansky, *Supergravity Workshop Stony Brook, New York, September 27-28, 1979*, Conf. Proc. **C790927**, 315 (1979), arXiv:1306.4669 [hep-th].
- [46] J. Schechter and J. W. F. Valle, Phys. Rev. **D22**, 2227 (1980).
- [47] M. Fukugita and T. Yanagida, Phys. Lett. B **174**, 45 (1986).
- [48] K. Kumekawa, T. Moroi, and T. Yanagida, Prog. Theor. Phys. **92**, 437 (1994), arXiv:hep-ph/9405337.
- [49] T. Asaka, K. Hamaguchi, M. Kawasaki, and T. Yanagida, Phys. Rev. D **61**, 083512 (2000), arXiv:hep-ph/9907559.
- [50] L. Lavoura, Phys. Lett. B **609**, 317 (2005), arXiv:hep-ph/0411232.
- [51] E. I. Lashin and N. Chamoun, Phys. Rev. D **78**, 073002 (2008), arXiv:0708.2423 [hep-ph].
- [52] W. Altmannshofer, S. Gori, M. Pospelov, and I. Yavin, Phys. Rev. Lett. **113**, 091801 (2014), arXiv:1406.2332 [hep-ph].
- [53] R. Harnik, J. Kopp, and P. A. N. Machado, JCAP **07**, 026 (2012), arXiv:1202.6073 [hep-ph].
- [54] S. Bilmis, I. Turan, T. M. Aliev, M. Deniz, L. Singh, and H. T. Wong, Phys. Rev. D **92**, 033009 (2015), arXiv:1502.07763 [hep-ph].

- [55] J. P. Lees *et al.* (BaBar), Phys. Rev. D **94**, 011102 (2016), arXiv:1606.03501 [hep-ex].
- [56] C. Patrignani *et al.* (Particle Data Group), Chin. Phys. C **40**, 100001 (2016).
- [57] I. Esteban, M. C. Gonzalez-Garcia, M. Maltoni, T. Schwetz, and A. Zhou, JHEP **09**, 178 (2020), arXiv:2007.14792 [hep-ph].
- [58] N. Aghanim *et al.* (Planck), Astron. Astrophys. **641**, A6 (2020), [Erratum: Astron.Astrophys. 652, C4 (2021)], arXiv:1807.06209 [astro-ph.CO].
- [59] A. M. Baldini *et al.* (MEG), Eur. Phys. J. C **76**, 434 (2016), arXiv:1605.05081 [hep-ex].
- [60] B. Aubert *et al.* (BaBar), Phys. Rev. Lett. **104**, 021802 (2010), arXiv:0908.2381 [hep-ex].
- [61] S. Abe *et al.* (KamLAND-Zen), arXiv preprint (2022), arXiv:2203.02139 [hep-ex].
- [62] M. Agostini *et al.* (GERDA), Phys. Rev. Lett. **125**, 252502 (2020), arXiv:2009.06079 [nucl-ex].
- [63] M. Escudero, D. Hooper, G. Krnjaic, and M. Pierre, JHEP **03**, 071 (2019), arXiv:1901.02010 [hep-ph].
- [64] A. Albert (ATLAS, CMS), PoS **LHCP2021**, 076 (2021).
- [65] T. Nomura and T. Shimomura, Eur. Phys. J. C **79**, 594 (2019), arXiv:1803.00842 [hep-ph].
- [66] B. Adhikary, Phys. Rev. D **74**, 033002 (2006), arXiv:hep-ph/0604009.
- [67] E. K. Akhmedov, V. A. Rubakov, and A. Yu. Smirnov, Phys. Rev. Lett. **81**, 1359 (1998), arXiv:hep-ph/9803255 [hep-ph].
- [68] T. Asaka and M. Shaposhnikov, Phys. Lett. **B620**, 17 (2005), arXiv:hep-ph/0505013 [hep-ph].
- [69] A. Pilaftsis and T. E. J. Underwood, Nucl. Phys. B **692**, 303 (2004), arXiv:hep-ph/0309342.
- [70] G. F. Giudice, A. Notari, M. Raidal, A. Riotto, and A. Strumia, Nucl. Phys. B **685**, 89 (2004), arXiv:hep-ph/0310123.
- [71] D. Borah, A. Dasgupta, and D. Mahanta, Phys. Rev. D **104**, 075006 (2021), arXiv:2106.14410 [hep-ph].
- [72] M. Abdullah, J. B. Dent, B. Dutta, G. L. Kane, S. Liao, and L. E. Strigari, Phys. Rev. D **98**, 015005 (2018), arXiv:1803.01224 [hep-ph].
- [73] S. N. Gninenko, N. V. Krasnikov, and V. A. Matveev, Phys. Rev. D **91**, 095015 (2015), arXiv:1412.1400 [hep-ph].
- [74] S. N. Gninenko and N. V. Krasnikov, Phys. Lett. B **783**, 24 (2018), arXiv:1801.10448 [hep-ph].

- [75] K. Abazajian *et al.*, arXiv preprint (2019), arXiv:1907.04473 [astro-ph.IM].
- [76] M. W. Winkler, Phys. Rev. D **99**, 015018 (2019), arXiv:1809.01876 [hep-ph].
- [77] S. Dittmaier *et al.* (LHC Higgs Cross Section Working Group), (2011), 10.5170/CERN-2011-002, arXiv:1101.0593 [hep-ph].